

1

2 **Centromere Innovations Within a Mouse Species**

3

4

5 Craig W. Gambogi^{1,2,3,4^}, Nootan Pandey^{1,2,3^}, Jennine M. Dawicki-McKenna^{1,2,3^},

6 Uma P. Arora^{5,6}, Mikhail A. Liskovskykh⁷, Jun Ma⁸, Piero Lamelza⁸, Vladimir Larionov⁷,

7 Michael A. Lampson⁸, Glennis A. Logsdon⁹, Beth L. Dumont^{5,6}, and Ben E. Black^{1,2,3,4*}

8

9 ¹Department of Biochemistry and Biophysics, Perelman School of Medicine, University of
10 Pennsylvania, PA 19104

11 ²Penn Center for Genome Integrity, University of Pennsylvania, Philadelphia, PA 19104

12 ³Epigenetics Institute, University of Pennsylvania, Philadelphia, PA 19104

13 ⁴Biochemistry and Molecular Biophysics Graduate Group, University of Pennsylvania,
14 Philadelphia, PA 19104

15 ⁵The Jackson Laboratory, Bar Harbor, ME 04609

16 ⁶Graduate School of Biomedical Sciences, Tufts University, Boston, MA 02111

17 ⁷Developmental Therapeutics Branch, National Cancer Institute, Bethesda, MD 20892

18 ⁸Department of Biology, University of Pennsylvania, Philadelphia, PA 19104

19 ⁹Department of Genome Sciences, University of Washington School of Medicine, Seattle, WA
20 98195

21

22 [^]equal contribution

23 *correspondence: blackbe@pennmedicine.upenn.edu

24

25

26

27 **Abstract**

28 Mammalian centromeres direct faithful genetic inheritance and are typically characterized by
29 regions of highly repetitive and rapidly evolving DNA. We focused on a mouse species, *Mus*
30 *pahari*, that we found has evolved to house centromere-specifying CENP-A nucleosomes at the
31 nexus of a satellite repeat that we identified and term π -satellite (π -sat), a small number of
32 recruitment sites for CENP-B, and short stretches of perfect telomere repeats. One *M. pahari*
33 chromosome, however, houses a radically divergent centromere harboring ~6 Mbp of a
34 homogenized π -sat-related repeat, π -sat^B, that contains >20,000 functional CENP-B boxes. There,
35 CENP-B abundance drives accumulation of microtubule-binding components of the kinetochore,
36 as well as a microtubule-destabilizing kinesin of the inner centromere. The balance of pro- and
37 anti-microtubule-binding by the new centromere permits it to segregate during cell division with
38 high fidelity alongside the older ones whose sequence creates a markedly different molecular
39 composition.

40

41 **Teaser**

42 Chromatin and kinetochore alterations arise in response to evolutionarily rapid changes to
43 underlying repetitive centromere DNA.

44

45 **Introduction**

46 Centromeres are the loci that coordinate chromosome segregation during cell division
47 (1). They do so by assembling a proteinaceous structure, the kinetochore, at cell division that
48 attaches to spindle microtubules, housing the chromatin that regulates microtubule attachment
49 to ensure error-free segregation, and serving as the final site of sister chromatid cohesion. In
50 many species, including mammals, the site for all of these functions is epigenetically specified by
51 the presence of nucleosomes harboring the histone H3 variant, CENP-A.

52 Despite generally shared and essential functional roles there is marked diversity in the
53 DNA sequences and molecular composition of centromeres between different eukaryotic
54 species. Centromere formation can influence evolution by allowing some centromeres to be
55 preferentially inherited during female meiosis by biasing segregation outcomes in a process
56 called 'centromere drive' or more generally 'meiotic drive' (2, 3). Centromeres that direct biased
57 segregation to the egg are referred to as 'stronger' centromeres. Among other factors,

58 expanding the region of DNA housing CENP-A nucleosomes can strengthen the centromere (4).

59 Female meiotic drive is thought to be the major driver of rapid evolution of centromeric DNA (5).

60 One powerful model system for assessing the molecular basis for female meiotic drive is
61 the mouse (6). Prior work has demonstrated that major differences in the abundance of
62 repetitive centromere DNA between inbred laboratory strains or species lead to differences in
63 which chromosomes are more likely to be inherited through meiosis (6). While centromere DNA
64 sequence and architecture differs between mouse species, in each of the reported cases,
65 centromere DNA differences between chromosomes within a strain or species are thought to be
66 negligible (e.g. every *Mus spreitus* chromosome has a nearly identical repeat at each centromere
67 at a similar abundance) (4, 7, 8). Of course, centromeres are present on separate chromosomes
68 implying that DNA sequence-based differences between centromeres are homogenized across
69 the genome through some undefined selective pressure to do so. More precisely, individual
70 chromosomes are physically unlinked and subject to the independent accrual of new mutations.
71 Non-allelic homologous repair processes can homogenize centromeres from different
72 chromosomes, erasing signals of chromosome-level centromere divergence (9, 10). Such
73 mechanisms have likely been particularly active on acrocentric mouse chromosome, where
74 centromeres colocalize at the nuclear periphery during meiosis onset, prior to the completion of
75 double-strand DNA break repair (11). Nonetheless, the rapid evolution of centromeric DNA
76 suggests that genomes with heterologous centromere composition are potentially pervasive,
77 even if only transiently manifest in mouse genomes.

78 Thus, evolutionary intermediates must have existed prior to homogenization, and the
79 molecular consequences remain unclear of having divergent centromeric DNA within a single
80 mouse strain and/or species. In other eukaryotes, there are examples of different centromeres
81 within a species, but it is unclear how they relate to the mouse model for strengthening through
82 modulation of DNA repeat number or sequence due to major differences at the centromere. For
83 instance, plant neocentromeres, like a famous example in maize (12–14) can function not
84 through an actual centromere/kinetochore but by directing independent movements through
85 tethering a specialized motor protein to the spindle. In mammals, evolutionarily young
86 centromeres have been found on up to half of the centromeres of individual equine species (15).
87 Further, many are present (albeit on smaller numbers of chromosomes) in several other
88 vertebrate systems (16–19). In all these documented cases, the young centromeres consist of
89 non-repetitive DNA. Given the recent successful studies using the mouse model system to reveal

90 the role of centromere strength in centromere evolution (4, 8, 20), advances in mice on isolating
91 and studying new radical changes in repetitive centromere DNA are likely to have important
92 implications for advancing models of centromere evolution in diverse eukaryotic species.

93 CENP-B is the only known sequence-specific DNA-binding protein found at many
94 eukaryotic centromeres, including at the centromeres in diverse mammalian species. It
95 recognizes a conserved 17-mer sequence termed the CENP-B box, in which 9 positions are
96 essential for CENP-B binding (21, 22). The CENP-B box is found within the sequences of the
97 centromere repeat monomers (i.e. within the 171 bp alpha-satellite repeat in *Homo sapiens* and
98 within the 120 bp repeat in minor satellite in *Mus. musculus*) (23, 24). While not essential for
99 centromere function (indeed CENP-B boxes are absent on the Y chromosome in humans and mice
100 (25)), CENP-B can buffer against other molecular insults and is a prime candidate to play a role in
101 modulating centromere strength (20, 25, 26). CENP-B serves to support the pericentromeric
102 enrichment of constitutive heterochromatin (i.e. chromatin enriched with nucleosomes marked
103 with histone H3 lysine 9 trimethylation [H3K9me3]) that, in turn, enhances the recruitment of
104 inner centromere components involved in sister chromatid cohesion and the process of mitotic
105 error correction (20, 27–29). CENP-B, likewise, enhances kinetochore formation through its
106 ability to bind an essential centromere protein, CENP-C (25). Removal of CENP-B enhances
107 functional differences in female meiosis between diverged strains of *M. musculus* that have
108 approximately ten-fold differences in minor satellite abundance relative to one another (20).
109 Thus, there is a strong support for the notion that CENP-B can play a key role in modulating
110 centromere strength.

111 Here, we find that CENP-B is dispensable for CENP-A nucleosome positioning on minor
112 satellite DNA, suggesting that its roles are likely limited to strengthening the centromere by other
113 proposed means that rely on the amount of CENP-B at the centromere. We then identify a single
114 chromosome in the mouse species *M. pahari* that has a massive expansion of a newly evolved
115 repeat array that houses >20,000 functional CENP-B boxes: ~100-fold more than on the other *M.*
116 *pahari* centromeres. Using a comprehensive set of short- and long-read sequencing-based
117 methodologies, we define this centromere and the more typical centromeres in *M. pahari*. The
118 latter accumulate kinetochore forming CENP-A chromatin at a subset of repeats that harbor a
119 relatively small number (hundreds) of CENP-B boxes, as well as up to 68,000 telomere repeats.
120 Taken together, our sequencing efforts predict a difference in the molecular composition of the
121 two types of centromeres within a single organismal genome. We test this notion and determine

122 how the opposing recruitment of microtubule-binding and microtubule-destabilizing factors co-
123 exist in the same mouse species.

124

125 **Results**

126 ***Positioning of CENP-A Nucleosomes on Minor Satellite is Independent of CENP-B***

127 In *M. musculus*, CENP-B boxes are only found within minor satellite DNA (30). CENP-A
128 nucleosomes predominantly occupy a single site within the minor satellite repeat, with their
129 centers (also known as the nucleosomal dyad) precisely positioned within the CENP-B box (4).
130 While this nucleosome position is used by conventional nucleosomes containing canonical
131 histone H3, it is only one of several prominent sites for CENP-A nucleosome assembly. In
132 principle, minor satellite DNA sequence could directly impact the position of CENP-A containing
133 nucleosomes independently of CENP-B binding. Alternatively, the CENP-B protein could impact
134 CENP-A nucleosome positioning upon binding to the CENP-B box and through its direct and
135 indirect interactions with the CENP-A nucleosomes. To distinguish between these possibilities,
136 we enriched for nucleosomes containing either CENP-A or H3K9me3 via chromatin
137 immunoprecipitation (ChIP) from chromatin isolated from wild type (WT; C57BL/6J) or CENP-B^{-/-}
138 (C57BL/6J) mice. We found that positioning on minor satellite of CENP-A nucleosomes, H3K9me3
139 nucleosomes, and the total pool of nucleosomes (input to the native ChIP) were essentially
140 unchanged in the absence of CENP-B protein (Fig. 1A, B). Thus, our data support the notion that
141 minor satellite DNA sequence is uniquely responsible for positioning of CENP-A nucleosomes,
142 independently of the presence of CENP-B protein. Our results suggest that CENP-B protein, the
143 CENP-B box, and centromere satellite sequences are important for us to consider in contributing
144 to centromere drive.

145

146 ***Rapid Centromere DNA Repeat Evolution Impacts the Amount of CENP-B at Centromeres***

147 Early hybridization studies indicate that closely related house mouse species are
148 undergoing evolutionarily rapid changes in centromere DNA sequence (Fig. 1C) (23, 31, 32). This
149 divergence can include the number of CENP-B boxes and/or the sequence of the repeat, itself
150 (33). One way to alter CENP-B box number is to vary the abundance of homogeneous centromere
151 repeats. For instance, in *M. spretus* minor satellite is the most abundant centromere satellite and
152 major satellite is much less abundant (23); the opposite of what is found in *M. musculus*. Changes

153 also include apparent drastic alterations in DNA sequence, as in *M. pahari* where major satellite
154 is undetectable (31, 32).

155 Two initial observations suggested that investigating the centromere diversity in *M.*
156 *pahari* could yield new insights into the mechanism governing centromere strength. First, the *M.*
157 *pahari* genome encodes the CENP-B protein which is almost identical to its counterpart in *M.*
158 *musculus* and 100% identical in its DNA-binding domain (Fig. 1D). Such high species-level protein
159 conservation is highly unlikely to persist over evolutionary time in the absence of purifying
160 selection to retain CENP-B function. Thus, we anticipated that *M. pahari* centromeres would
161 contain repeats—minor satellite DNA or other divergent repetitive centromere DNA—that
162 harbor functional CENP-B box sequences capable of CENP-B binding. Second, we found that while
163 most *M. pahari* centromeres have low (relative to those from *M. musculus* cells co-seeded for
164 immunofluorescence measurements) yet detectable levels of CENP-B, a pair of very strong foci
165 of CENP-B are present (Fig. 1E). We concluded that the pair of foci likely represent a single pair
166 of homologous chromosomes. Thus, our initial observations suggested that in *M. pahari*, major
167 changes exist in centromere DNA both relative to *M. musculus* and between different *M. pahari*
168 chromosomes and that impacts the CENP-B abundance at the centromeres.

169

170 ***Identification of a Divergent Centromere Satellite, π -sat***

171 Since no centromere satellite has been identified in *M. pahari*, we employed several
172 strategies to identify candidate centromere repeats (Fig. 2A). The first strategy was a *k*-mer-
173 based approach using an existing short-read sequencing data set (34). This yielded a top hit with
174 a repeat unit length of 189 bp (Fig. S1). The second strategy was an analysis of total nucleosomal
175 DNA and CENP-A nucleosome-enriched (native ChIP) short-read data with the computational
176 pipeline TAREAN (35) coupled to downstream analysis of native Oxford Nanopore Technologies
177 (ONT) long-read sequencing we performed of the *M. pahari* genome (Fig. 2A; see Methods for
178 details of the strategy we employed). This produced a total of three sequences with a high
179 likelihood of satellite DNA (Fig. 2B; Methods). Of the three sequences, the 189 bp satellite, which
180 we term π -sat, is nearly identical to the top hit identified by the *k*-mer strategy (Fig. S1).
181 Consistent with our hypothesis that is a centromere repeat, π -sat hybridizes to a single locus on
182 each chromosome in a chromosome spread of mitotic *M. pahari* cells (Fig. 2C). However, the π -
183 sat sequence lacks an intact CENP-B box (Fig 2D). The two remaining repeats we identified are

184 related to π -sat: one (π -sat^{sh}) is ~50 bp shorter, whereas the other (π -sat^B) contains an intact
185 CENP-B box (Fig. 2D).

186 We noted that none of the three π -satellites we identified were closely related to major
187 satellite from *M. musculus*, explaining why early hybridization studies failed to identify major
188 satellite in *M. pahari* (31, 32). Minor satellite similarly has only small regions of identity with π -
189 sat, and the region of π -sat aligning to the CENP-B box has several substitutions (Fig. 2E).
190 Alignment of enriched sequences from CENP-A (functional centromere) and H3K9me3 (enriched
191 in pericentromeric heterochromatin) native ChIP with π -sat yielded strong peaks of high
192 sequence identity (Fig. 2F). Further, we noted that many of the long-reads that align to π -sat
193 consisted of homogenous stretches where π -sat contained no intervening sequences, including
194 any π -sat^{sh} or π -sat^B (Fig. 2G). Together with the FISH and native ChIP data, these experiments
195 suggest that most or all *M. pahari* centromeres harbor long and uninterrupted stretches of π -sat
196 repeats that lack functional CENP-B boxes.

197

198 ***A Chromosome Pair with Highly Homogenized π -sat^B***

199 To gain an understanding of the centromere sequences that harbor functional CENP-B
200 boxes, we employed another strategy (Fig. 3A), starting with native ONT long reads that harbor
201 functional CENP-B box sequences. This approach yielded a refined centromere consensus
202 sequence (Fig. 3B) that corresponded to what we had initially identified as π -sat^B (Fig. 2). CENP-
203 A and H3K9me3 native ChIP reads contained many sequences that align well to the π -sat^B
204 consensus sequence (Fig. 3C). Peaks around 83-86% sequence identity likely correspond to
205 alignments with general π -sat, while a peak around 94-96% sequence identity likely represents
206 π -sat^B sequences. We designed a FISH probe using the π -sat^B consensus sequence and found that
207 it hybridized to a pair of mitotic chromosomes in *M. pahari* cells (Fig. 3D). Further, in interphase
208 *M. pahari* cells the π -sat^B probe colocalized with a probe specific to the CENP-B box (Fig. S2). This
209 supported our prior conclusion that the two nuclear puncta with high amounts of CENP-B (Fig.
210 1E) correspond to a single pair of homologous chromosomes. Alignment of sequences found on
211 long reads containing either π -sat or π -sat^B showed that π -sat^B has near invariance at the CENP-
212 B box positions that are required for CENP-B binding, including at the positions that diverge from
213 the π -sat consensus (Fig. 3E). The majority of ONT long reads containing centromere repeats were
214 homogenous stretches that align more closely to π -sat and were devoid of CENP-B boxes. On the
215 other hand, a smaller proportion contain centromere repeats that, while also comprising

216 homogenous stretches, contain many functional CENP-B boxes and align more closely to π -sat^B
217 (Fig. 3F). Our findings indicate that a homologous pair of chromosomes that bind high levels of
218 CENP-B harbor a large and highly homogenous derivative of the satellite present on the other
219 chromosomes.

220

221 ***High-accuracy Sequence Assemblies of *M. pahari* Centromeres***

222 In order to identify the chromosome with high amounts of CENP-B, as well as to more
223 broadly understand centromere structure in *M. pahari*, we set out to generate centromere
224 sequence assemblies from several *M. pahari* chromosomes. While murine centromeres have long
225 been assumed to be relatively intractable to sequence assembly due to high repeat homogeneity
226 and apparent lack of higher-order repeat patterns (e.g., this is true of the best known murine
227 centromere repeat for centromere function in cell division, minor satellite from *M. musculus*),
228 we were encouraged by two aspects. The first was the success of Pacific Biosciences high-fidelity
229 (Pacbio HiFi) long-read sequencing in assembling human centromeres with high accuracy (36–
230 38). The second was our finding that π -sat is not as homogenous as minor satellite (Fig. 2G). Our
231 initial focus for sequence assembly was of the chromosome containing a large array of π -sat^B (Fig.
232 4A). Therefore, we generated a 22-fold coverage of PacBio HiFi data from the *M. pahari* genome
233 and assembled it with the whole-genome assembler hifiasm (39). This generated a whole-
234 sequence assembly that was 4.54 Gbp in length, consistent with its diploid nature, and containing
235 a contiguous assembly from the telomere through the first 13 Mbp of the chromosome
236 containing arrays of π -sat^B. Aligning this contig to an adjacent contig was sufficient to extend to
237 complex sequence that matches chromosome 11 from the initial genome build of *M. pahari* (34).
238 This chromosome is telocentric, with no intervening sequence between perfect telomere repeats
239 and centromeric repeats (Fig. 4A).

240 The first centromere repeats consist of a ~6 Mbp block of contiguous π -sat^B. The first 3.7
241 Mbp of this π -sat^B array includes monomers in exclusive head-to-tail orientation. The
242 directionality of the head-to-tail repeats switches three times over the next 2.3 Mbp. In total, this
243 6 Mbp block houses 21,617 functional CENP-B boxes (Fig. 4A) explaining the massive enrichment
244 of CENP-B on this chromosome (Fig. 1E). A ~4 Mbp contiguous stretch of π -sat lies distal to the
245 π -sat^B arrays, followed by a shorter stretch of π -sat variant, π -sat^{tel} (Fig. 5F). π -sat^{tel} is a more
246 complex composite repeat monomer comprised of elements built from π -sat, π -sat^{sh}, and 2-16
247 telomere repeats. CENP-A association is not uniform across the chromosome 11 centromere,

248 with enrichment localized to three sites: a site of enrichment adjacent to the telomere (0-250
249 kbp) and two more regions marked by peaks at ~750 kbp and 2.5 Mbp from the telomere,
250 respectively (Fig. 4A). CENP-A peaks are only observed on π -sat^B, but not on π -sat or π -sat^{tel} (Fig.
251 4A). Southern blots of *M. pahari* DNA digested with two restriction enzymes, BstXI and HpaI, and
252 probed with π -sat^B almost perfectly match the pattern predicted by our assembly (Fig. 4B). Two
253 predicted bands (183 and 650 kb) for BstXI digestion were not detected, but one at 833 kb was
254 (Fig. 4B). This minor difference is likely due to a sequence polymorphism between the animal
255 used to generate the assembly versus the one used to harvest DNA for the blot. Thus, despite the
256 high degree of sequence identity between repeat monomers and the lack of other unique
257 sequences for a >6 Mbp span of π -sat^B, our approach with PacBio HiFi long read sequencing
258 downstream assembly strategy is extremely faithful.

259 We successfully assembled seven other *M. pahari* centromeres (Fig. 5A-D, S4). Note, all
260 seven have unmapped regions between the centromere and the rest of the chromosome that
261 preclude assignment to a particular *M. pahari* chromosome, so we have numbered them
262 centromere (i)-(vii). They vary in size and precise arrangement, are commonly telocentric, and
263 house π -sat^{tel} between the telomere and a long stretch of π -sat (Fig. 5A-D, S4). Importantly, none
264 contain π -sat^B (Fig. 5A-D, S4). CENP-A peaks are almost entirely restricted to π -sat^{tel}, as are
265 functional CENP-B boxes (Fig. 5A-D, S4). The functional CENP-B boxes are almost exclusively
266 confined to π -sat^{tel} repeats and vary in their sequence from those found on chromosome 11 in
267 π -sat^B and are much less abundant (Fig. 5A-D, S3, S4). The majority of the π -sat repeats harbor
268 non-functional CENP-B boxes that do not match the consensus required for CENP-B binding (Fig.
269 5A-D, S4). Thus, other assembled centromeres harbor 27-143 times fewer total functional CENP-
270 B boxes than chromosome 11. For all centromeres that we assembled, the major site of CENP-A
271 enrichment spans 100-300 kbp (Fig. 5A-D, S4). As far as the role of the different specific forms of
272 π -sat, general π -sat is the most abundant and represent a candidate pericentromeric satellite
273 (analogous to major satellite DNA in *M. musculus*), while both π -sat^{tel} and π -sat^B are primary sites
274 for kinetochore forming chromatin containing CENP-A nucleosomes (Fig. 5E). Compared to
275 chromosome 11, the other centromeres contain π -sat wherein monomer units are less similar to
276 one another (Fig. 3F). Thus, it appears that the highly homogenous chromosome 11 centromere
277 is evolutionarily more recent. In total, our long-read analysis of *M. pahari* centromeres define the
278 general sequence features of *M. pahari* centromeres, including the evolutionary young
279 centromere on chromosome 11.

280

281 ***Co-existence of Chromosomes with Markedly Different Abundance of Centromere Factors***

282 Chromosome 11 has a markedly different centromere repeat that leads to massive
283 differences in CENP-B abundance (Fig. 4A). To test whether or not the large difference of CENP-
284 B leads to higher levels of H3K9me3 accumulation, we performed quantitative
285 immunofluorescence on interphase cells (Fig. 6A,B). Indeed, chromosome 11 has 1.6-fold higher
286 H3K9me3 relative to that measured at the centromeres of other chromosomes have low yet
287 detectable CENP-B levels (Fig. 6A,B).

288 Differences in centromere repeats between different mouse strains and species also have
289 downstream molecular consequences that direct changes in the abundance of factors involved
290 in microtubule-attachment (i.e. microtubule-binding proteins of the kinetochore, such as
291 Hec1^{Ndc80}) or in microtubule-destabilization (i.e. the kinesin, MCAK, that uses its motor activity to
292 disassemble kinetochore microtubules) (4, 7, 8). The *M. pahari* genome harbors chromosomes
293 with divergent centromere architectures that must undergo mitosis in unison and therefore it
294 presents a unique opportunity for investigating the regulation of microtubule dynamics at the
295 kinetochore. One likely scenario we considered is that the molecular changes yield a similar
296 balance of microtubule couplers (e.g. Hec1^{Ndc80}) and destabilizers (e.g. MCAK), so that their ratio
297 is similar enough to each align and segregate on the mitotic spindle with similar fidelity. Current
298 models suggest that CENP-B recruits MCAK is thought to be via its role in enriching H3K9me3
299 chromatin. Per our expectation, we observed an approximately 1.8-fold enrichment of MCAK on
300 chromosome 11 relative to the other *M. pahari* chromosomes during mitosis (Fig. 6C,D). Thus, the
301 heterochromatin pathway governing centromere strength leads to greater accumulation of a
302 primary microtubule-destabilizer on chromosome 11. We hypothesized that the kinetochore
303 pathway stimulated by CENP-B would likely be impacted, as well. To measure this, we detected
304 the kinetochore microtubule coupler Hec1^{Ndc80}, and found it, too, is recruited on 1.2-fold higher
305 levels on chromosome 11 than on other chromosomes (Fig. 6E,F).

306 Since there are both increased levels of MCAK and Hec1^{Ndc80} on chromosome 11, we
307 predict that this chromosome will properly segregate at rates comparable to the other *M. pahari*
308 chromosomes. In unperturbed cells, chromosome segregation errors lead to a small percentage
309 (1.5 +/- 0.14% in our experiment) of cells having micronuclei. This is increased to 4.2 +/- 0.91% in
310 our experiment by transient incubation with the microtubule poison, nocodazole. In both cases,

311 chromosome 11 missegregation to micronuclei (Fig. 6G-I) is near the expected value if there is
312 no bias simply based on chromosome number (Fig. 6I, dashed grey line). Note, the slightly higher
313 than expected value is explained by a likely undercount of the other chromosomes that are
314 present in micronuclei since their levels of CENP-B which is used to identify missegregated
315 chromosomes are lower than on chromosome 11. Together, our cell-based measurements
316 support the notion that despite chromosome 11 having different centromere DNA, its
317 segregation fidelity is the same relative to the remaining centromeres.

318

319 **Discussion**

320 For rapid centromere evolution to occur, a new innovation within a species would have
321 to initiate on a single chromosome. Some innovations will strengthen centromeres and spread
322 to other chromosomes, eventually becoming the dominant form within a species. We have
323 identified and characterized a new repeat, π -sat^B, in *M. pahari* that exists as a homogenous 6
324 Mbp array that confers centromere function on chromosome 11. The chromosome 11
325 centromere is an outlier compared to centromeres in other species. In *M. musculus*, all
326 centromeres have similar numbers of CENP-B boxes and even in *H. sapiens* where centromeric
327 sequence diverge, the range of CENP-B box numbers varies only ~10 fold between chromosomes
328 (36, 38). On the other hand, chromosome 11 has 27-143 times more CENP-B boxes than
329 presumably evolutionarily older centromeres in *M. pahari* that we sequenced and assembled.
330 The chromosome 11 centromere directly recruits high levels of CENP-B that, in turn, generates a
331 larger kinetochore (Fig. 6E,F,7A). If not counterbalanced by corresponding increase in
332 microtubule-destabilization, such an innovation would likely lead to mitotic chromosome
333 segregation errors (Fig. 7B). We predict that other evolutionary instances of centromere
334 innovation would require similar or analogous counterbalancing of these opposing molecular
335 pathways during mitotic chromosome segregation, since imbalances are known to drive errors
336 in mitotic chromosome segregation (40). Invasion of stronger centromere sequences into other
337 chromosomes is likely to lead to imbalances during female meiosis that would favor the biased
338 segregation of the new centromeres into the egg. Such a model would put female meiosis as the
339 driver of the rapid expansion of new, stronger centromere sequences through an entire genome.
340 Testing this model with *M. pahari* will require the identification (and/or isolation) of strains or
341 closely related species where interspecies crosses produce viable animals with functional oocytes

342 [note that *M. pahari* does not productively mate with *M. musculus* or *M. spretus* (unpublished
343 observations, M.A.La.)]. Our study also opens up the prospect that other experimentally tractable
344 model systems exist where centromere innovation similarly initiates from one specific
345 chromosome.

346 To understand the arrangement of *M. pahari* centromeres, including the location of
347 CENP-A nucleosomes, we started with information from short-read sequencing. In the final
348 analysis, however, clarity on the situation would never have been achieved without employing
349 long-read sequencing that yielded complete centromere assemblies. Our approach was modeled
350 after the recent success in human centromere assemblies that has been a centerpiece
351 accomplishment of the Telomere-to-Telomere consortium (36–38). Our work exemplifies how
352 these approaches can be successfully employed to identify new centromere repeats in a non-
353 traditional model system (such as *M. pahari* that has had only modest genomic resources) for
354 understanding mammalian chromosome evolution. Further, it succeeded in assembling
355 centromeres harboring several megabases of repetitive DNA that are even more homogeneous
356 in sequence than are human centromeres. For the older, more numerous *M. pahari* centromeres,
357 our experiments revealed a association between CENP-A accumulation and repeats containing
358 short spans of perfect telomere sequences as well as CENP-B boxes (Fig. 5). This suggests that for
359 most centromeres in this species, the genetic contribution to centromere identity is particularly
360 high. On the other hand, within the 6 Mbp of the most homogenous repeat, π -sat^B on
361 chromosome 11, there is no strong sequence correlation with the specific peaks of CENP-A
362 enrichment, since the sequences are almost identical at sites of either high or low CENP-A
363 enrichment (Fig. 4A). It should be noted, though, that on chromosome 11 the highest peak of
364 CENP-A enrichment is also adjacent to the telomere repeats at the natural telomere (Fig. 4). The
365 lack of DNA sequence differences within the chromosome 11 centromere would suggest a strong
366 epigenetic feedback that organizes the functional centromere at discrete sites within a large ‘sea’
367 of homogenized DNA repeats. Similar observations have been made in *M. spretus* (and *M.*
368 *musculus*) where large stretches of homogenous centromeric DNA contain different kinds of
369 chromatin at discrete locations despite no apparent sequence differences (41). On a technical
370 note, our findings indicate that current sequencing methodologies and sequence assembly
371 approaches can tackle some of the longest stretches of the most homogenized centromere
372 sequences known in biology. Thus, massive stretches of similarly repetitive regions in other

373 species (i.e. major satellite in *M. musculus*) should now be feasibly assembled using these
374 methodologies.

375 Rapid centromere evolution is thought to be tied to karyotypic changes that separate
376 closely related species (42–46). On one hand, the position (i.e. telocentric versus metacentric),
377 size, and sequence of centromere DNA is malleable, since closely related species harbor striking
378 changes between these attributes (43, 46). On the other hand, centromere repeats are generally
379 homogenized within a species (44), supporting the concept that there is a positive functional
380 consequence of having similar centromere function (i.e. recruitment of similar amounts of
381 centromere proteins) across centromeres within a single species. The example in this study of *M.*
382 *pahari*, shows how radical functional change to one of these attributes (centromere repeat) can
383 be tolerated through counterbalancing pro-and anti-attachment of the centromere to spindle
384 microtubules during cell division. We propose that the selective force to counterbalance
385 functional centromere strength properties within a species shapes the nature and magnitude of
386 innovations that would have the chance to ‘take hold’ in a population during the evolution of
387 centromeres.

388

389 **Methods**

390 ***Experimental Model and Subject Details***

391 ***Mice***

392 Mouse strains were purchased from the Jackson Laboratory (C57BL/6J # 000664 and
393 PAHARI/EiJ # 002655). The CENP-B wild-type and knock-out mouse lines were generated as
394 described previously (20). *M. pahari* used for ChIP were male and the age was 6 months. CENP-
395 B WT/KO mice were female, and the age was 3.5 months. All animal experiments were approved
396 by the Institutional Animal Care and Use Committee and were consistent with the National
397 Institutes of Health guidelines.

398

399 ***Cell lines***

400 Primary lung fibroblasts were isolated from *M. musculus* or *M. pahari* as described
401 previously (47). Cells were immortalized by transfection of SV40 large T antigen (48) a gift from
402 Dr. B. Johnson (Upenn) using TransIT-X2 Dynamic Delivery System (Mirus). T-antigen integration
403 was confirmed by PCR (5'-GGAATCTTGCAGCTAATGGACCTTC-3' and 5'-
404 CCTCCAAAGTCAGGTTGATGAGCA-3' primers yield a 246 bp product).

405

406 **Cell culture**

407 The immortalized mouse primary fibroblasts were cultured in Dulbecco's Modified Eagle
408 medium (DMEM/F-12) supplemented with 10% FBS (Sigma), 1% penicillin–streptomycin (Gibco)
409 at 37°C in a humidified atmosphere with 5% CO₂.

410

411 **Primary mouse embryonic fibroblasts cultures**

412 Mouse embryonic fibroblasts (MEFs) lines were isolated from a pregnant female E12.5–
413 E13.5 embryos from *M. pahari* (PAHARI/Eij). MEFs were cultured in MEF media composed of
414 Dulbecco's Modified Eagle medium (DMEM) supplemented with 10% FBS (Lonza), 100 µg/mL
415 Primocin (Invivogen), and 1x GlutaMAX (Thermo Fisher Scientific/GIBCO) at 37°C in a humidified
416 atmosphere with 5% CO₂.

417

418 **Method Details**

419 **MNase-digested chromatin and native ChIP**

420 ChIP was performed as described previously (4). Briefly, nuclei were isolated from flash-
421 frozen mouse livers. Livers were homogenized in 4 mL ice-cold Buffer I (0.32 M sucrose, 60 mM
422 KCl, 15 mM NaCl, 15 mM Tris-Cl, pH 7.5, 5 mM MgCl₂, 0.1 mM EGTA, 0.5 mM DTT, 0.1 mM PMSF,
423 1 mM leupeptin/pepstatin, 1 mM aprotinin) per g of tissue by dounce homogenization.
424 Homogenate was filtered through 100 µm cell strainer (Falcon) and centrifuged at 6000 × g for
425 10 min at 4°C. The pellet was resuspended in the same volume Buffer I. An equivalent volume
426 ice-cold Buffer I supplemented with 0.2% IGEPAL was added, and samples were incubated on ice
427 for 10 min. 4 mL nuclei were layered on top of 8 mL ice-cold Buffer III (1.2 M sucrose, 60 mM KCl,
428 15 mM NaCl, 5 mM MgCl₂, 0.1 mM EGTA, 15 mM Tris, pH 7.5, 0.5 mM DTT, 0.1 mM PMSF, 1 mM
429 leupeptin/pepstatin, 1 mM aprotinin) and centrifuged at 10,000 × g for 20 min at 4°C with no
430 brake. Pelleted nuclei were resuspended in Buffer A (0.34 M sucrose, 15 mM HEPES, pH 7.4, 15
431 mM NaCl, 60 mM KCl, 4 mM MgCl₂, 1 mM DTT, 0.1 mM PMSF, 1 mM leupeptin/pepstatin, 1 mM
432 aprotinin), flash-frozen in liquid nitrogen, and stored at –80°C. Nuclei were digested with MNase
433 (Affymetrix) using 0.05–0.15 U/µg chromatin in Buffer A supplemented with 3 mM CaCl₂ for 10
434 min at 37°C. The reaction was quenched with 10 mM EGTA on ice for 5 min and an equal volume
435 of 2× Post-MNase Buffer (40 mM Tris, pH 8.0, 220 mM NaCl, 4 mM EDTA, 2% Triton X-100, 0.5
436 mM DTT, 0.5 mM PMSF, 1 mM leupeptin/pepstatin, 1 mM aprotinin) was added prior to

437 centrifugation at 18,800 \times g for 15 min at 4°C. The supernatant containing the MNase-digested
438 chromatin was pre-cleared with 100 μ L 50% Protein G Sepharose bead (GE Healthcare) slurry in
439 1x Post-MNase Buffer for \sim 2 hours at 4°C with rotation. Beads were blocked in NET Buffer (150
440 mM NaCl, 50 mM Tris, pH 7.5, 1 mM EDTA, 0.1% IGEPAL, 0.25% gelatin, and 0.03% NaN₃). Pre-
441 cleared supernatant was divided so that an estimated 250 μ g chromatin was used for ChIP 10 μ g
442 H3K9me3 antibody (Abcam ab8898) or 10 μ g anti-mouse specific CENP-A antibody, (custom-
443 made by Covance and affinity-purified in-house) and 12.5 μ g was saved as input. The custom
444 polyclonal antibody raised against mouse CENP-A. Briefly, a New Zealand White rabbit was
445 immunized using purified GST-tagged mouse CENP-A (aa 6-30) in PBS as an antigen and Freund's
446 adjuvant. ChIP samples were rotated at 4°C for 2 hours. Immunocomplexes were recovered by
447 addition of 100 μ L 50% NET-blocked protein G Sepharose bead slurry followed by overnight
448 rotation at 4°C. The beads were washed three times with wash Buffer 1 (150 mM NaCl, 20 mM
449 Tris-HCl, pH 8.0, 2 mM EDTA, 0.1% SDS, 1% Triton X-100), once with high salt Wash buffer (500
450 mM NaCl, 20 mM Tris-HCl, pH 8.0, 2 mM EDTA, 0.1% SDS, 1% Triton X-100), and the chromatin
451 was eluted 2 \times each with 200 μ L Elution Buffer (50 mM NaHCO₃, 0.32 mM sucrose, 50 mM Tris,
452 pH 8.0, 1 mM EDTA, 1% SDS) at 65°C for 10 min at 1500 rpm. The input sample was adjusted to
453 a final volume of 400 μ L with Elution Buffer. To each 400 μ L input and ChIP sample, 16.8 μ L of 5
454 M NaCl and 1 μ L of RNase A (10 mg/mL) was added. After 1 hour at 37°C, 4 μ L of 0.5M EDTA and
455 12 μ L Proteinase K (2.5 mg/mL, Roche) were added, and samples were incubated for another 2
456 hours at 42°C. The resulting Proteinase-K treated samples were subjected to a phenol-chloroform
457 extraction followed by purification of DNA with a QiaQuick PCR Purification column (Qiagen) in
458 preparation for high-throughput sequencing.

459

460 ***High-throughput sequencing***

461 Purified, unamplified input or ChIP DNA (see section MNase-digested chromatin and
462 native ChIP) was quantified using an Agilent 2100 Bioanalyzer high sensitivity kit. DNA libraries
463 were prepared for multiplexed sequencing according to Illumina recommendations as described
464 (49) with minor modifications using NEB enzymes. Briefly, 5 ng input or ChIP DNA was end-
465 repaired and A-tailed. Illumina TruSeq adaptors were ligated, libraries were size-selected to
466 exclude polynucleosomes, and adapter-modified DNA fragments were enriched by PCR using
467 KAPA polymerase. Libraries were assessed by Bioanalyzer and the degree of nucleosome
468 digestion for each experiment was assessed to avoid any potentially over-digested samples.

469 Libraries were submitted for 150 bp, paired-end Illumina sequencing on a NextSeq 500
470 instrument.

471

472 ***Paired-end sequencing analysis***

473 Paired-end sequencing analysis was performed as described previously (4). Briefly, paired-end
474 reads were converted to a name-sorted SAM file using picard-tools and samtools (50) then joined
475 in MATLAB using the ‘localalign’ function to determine the overlapping region between the
476 paired-end reads [requiring $\geq 95\%$ overlap identity; (49)], and adapter sequences were removed
477 if present. For analysis of minor and major satellite DNA, we used a custom tandem repeat
478 analysis as described (49) with the following modifications. Joined reads were aligned to a
479 trimerized mouse minor satellite consensus (GenBank: X14464.1) (30) or dimerized π -sat
480 consensus or to the reverse complement of those tandem consensus sequences. Those joined
481 reads aligning with $\geq 80\%$ identity were chosen for further analysis. To calculate the percent of
482 total reads, the number of joined reads aligning to the consensus sequence in either the forward
483 or reverse complement orientation (without double-counting any joined read) was divided by
484 the total number of joined reads. ChIP fold-enrichment was calculated as the fraction of reads
485 mapping to minor satellite from the ChIP divided by the fraction of reads mapping to minor
486 satellite in the input. Alignment of satellites was visualized with Matlab scripts
487 Code3_plotting_fixIncrement_1sizeClass_JDM20170206_allPlots or 2020-04-29-INP-consensus-
488 align-hist-line. Logo’s were generated via Glam2 with the command (glam2 -2 -a 190 -b 220 n
489 pahari_input_all_to_2nd_pisat_read.CENPBbox.10reads.fa -o 2nd_pisat_region_CBBox_10)
490 (51). Sequence alignments were generated using CLC Sequence Viewer.

491

492 ***TAREAN***

493 Putative satellite sequences were identified with TAREAN (35) from Illumina input
494 sequencing data (500,000 paired-end reads). Quality filtered and interlaced input fasta files were
495 prepared from fastq files as recommended. TAREAN was run with the following parameters:
496 cluster merging performed, no custom repeat database, cluster size threshold 0.0, no automatic
497 filtering of abundant repeats, similarity search options: Illumina reads, read length 100 nt or
498 more.

499

500 ***ONT long-read sequencing of the *M. pahari* genome***

501 To generate Oxford Nanopore Technologies (ONT) long-read sequencing data from the
502 *M. pahari* genome, we first extracted high-molecular weight DNA from ~2.5 million *M. pahari*
503 liver nuclei by resuspending them in 1 mL of Puregene Cell Lysis Solution (Cat. # 158113) in a 2
504 mL microfuge tube. Then, we added 6 μ L RNase A solution (Cat. # 158153) and incubated the
505 mixture at 37°C for 40 min. We let the mixture cool to room temperature before adding 333 μ L
506 of Puregene Protein Precipitation Solution (Cat. # 158123), vortexing for 20 sec, and then placing
507 the tube on ice for 10 min. We spun the tube containing the mixture at maximum speed in a 4°C
508 microfuge for 3 min. Then, we split the supernatant into two separate 1.5 mL tubes with 700 μ L
509 in each. We added 750 μ L isopropanol to each tube, inverted 50 times to mix, and then spun the
510 tubes at maximum speed in a 4°C microfuge for 1 min. We discarded the supernatant and then
511 added 666 μ L 70% ethanol to one of the tubes. We vortexed the single tube for 1 second and
512 then transferred all of the ethanol solution plus the pellet into the second tube. We vortexed
513 the second tube for 1 second and then spun at maximum speed in a 4°C microfuge for 1 min. We
514 washed the pelleted DNA with 666 μ L 70% ethanol two more times (pouring off the supernatant,
515 adding new 70% ethanol, briefly vortexing, and then spinning at maximum speed in a 4°C
516 microfuge for 1 min). After the second wash, we removed as much ethanol as possible from the
517 tube and let it air-dry for 25 min, until all traces of ethanol were gone. We then added 110 μ L of
518 Qiagen's DNA Hydration Solution (Cat. # 158133) to the DNA pellet and stored it at 4°C for two
519 days. Once the DNA was fully resuspended, we prepared the DNA for ONT long-read sequencing
520 using the ONT ligation sequencing kit (Cat. # SQK-LSK109), following the manufacturer's
521 instructions. The library was loaded onto a primed FLO-MIN106 R9.4.1 flow cell for sequencing
522 on the GridION. All ONT data was basecalled with Guppy 3.6.0 with the HAC model.

523

524 ***PACBio HiFi Sequencing of the *M. pahari* genome***

525 DNA extraction, library preparation, quality control, and sequencing were performed by
526 the Genome Technologies Scientific Service at The Jackson Laboratory. Approximately 60 μ g of
527 high molecular weight DNA was isolated from spleen tissue of a single *M. pahari* (PAHARI/EiJ)
528 male using the Monarch HMW DNA (NEB) according to the manufacturer's protocols with 2000
529 rpm agitation speed. DNA concentration and quality were assessed using the Nanodrop 2000
530 spectrophotometer (Thermo Scientific; 434 ng/ μ L), the Qubit 3.0 dsDNA BR Assay (Thermo
531 Scientific; 406 ng/ μ L), and the Genomic DNA ScreenTape Analysis Assay (Agilent Technologies).
532 DNA quality was assessed to be high (260/280 = 1.83, 260/230 = 2.29) and suitable for input for

533 PacBio HiFi library construction. A PacBio HiFi library was constructed using the SMRTbell Express
534 Template Prep Kit 2.0 (Pacific Biosciences) according to the manufacturer's protocols. Briefly, the
535 protocol entails shearing DNA using the g-TUBE (Covaris), ligating PacBio specific barcoded
536 adapters, and size selection on the Blue Pippin (Sage Science). The quality and concentration of
537 the library were assessed using the Femto Pulse Genomic DNA 165 kb Kit (Agilent Technologies)
538 and Qubit dsDNA HS Assay (ThermoFisher), respectively, according to the manufacturers'
539 instructions. The resultant library was sequenced on two SMRT cells on the Sequel II platform
540 (Pacific Biosciences) using a 30 hours movie time. The two SMRT cells yielded 71.25 and 93.94
541 Gb of unique sequence data, respectively, with an average read length of 13.9 kb.

542

543 ***Assembly of the *M. pahari* genome***

544 We assembled the *M. pahari* genome using PacBio HiFi data and the whole-genome
545 assembler, hifiasm [v0.16.1; (39)] using standard parameters. The assembled contigs were not
546 scaffolded into the entire chromosomes.

547

548 ***Alignment of CENP-A ChIP-seq and bulk nucleosomal data to the *M. pahari* genome assembly***

549 To identify the location of centromeric chromatin, we took advantage of the *M. pahari*
550 CENP-A ChIP-seq and bulk nucleosomal (input) data that we had generated. We first assessed the
551 reads for quality using FastQC (<https://github.com/s-andrews/FastQC>), trimmed them with Sickle
552 (<https://github.com/najoshi/sickle>) to remove low-quality 5' and 3' end bases, and trimmed them
553 with Cutadapt (52) to remove adapters. We aligned the processed CENP-A ChIP-seq reads to the
554 whole-genome *M. pahari* assembly using BWA (v0.7.17) with the following parameters: bwa
555 mem -t {threads} -k 50 -c 1000000 {path_to_index} {path_to_read1.fastq} {path_to_read2.fastq}.
556 We filtered the resulting SAM file to remove partial and supplementary alignments (retaining
557 only primary alignments) with SAMtools flag-F4 before normalizing the data to the input data
558 using DeepTools (v3.4.3) and the following command: bamCompare -b {path_to_CENP-A.bam} -
559 b2 {path_to_input.bam} --operation ratio --binSize 5000 --minMappingQuality 60 -p 20 -o
560 {out.bw}.

561

562 ***Identifying CENP-B boxes and telomere repeats within the *M. pahari* sequence assembly***

563 To identify the location of CENP-B boxes within the *M. pahari* genome assembly, we used
564 a custom python script (findKmers.py) to detect the location of the following sequences within

565 the assembly: 5'-TTCGNNNNANNCGGG-3' (the 17-bp CENP-B box) and 5'- CCCGNNTNNNNCGAA-
566 3' (the reverse-complement of the 17-bp CENP-B box) or 5'-TTAGGG-3' (telomere repeat) and 5'-
567 CCCTAA-3' (reverse complement of the telomere repeat). We ran the script with the following
568 command: ./findKmers.py --kmers {CENP-B_box_sequences} --fasta {genome_assembly.fasta} --
569 out {out.bed}/. We visualized the resulting BED file on the UCSC genome browser with the *M.*
570 *pahari* reference genome assembly.

571

572 ***Metaphase chromosome spreads of MEFs, FISH, and image capture***

573 FISH images of metaphase spreads of *M. pahari* cells were obtained using two different
574 protocols. To obtain FISH images of π -sat, MEFs were cultured in MEF media to \sim 80% confluence
575 at 37°C in a humidified atmosphere with 5% CO₂. Cells were subsequently serum starved on MEF
576 media without FBS and exposed to 0.02 μ g/mL Colcemid (Thermo Fisher Scientific/GIBCO) for 12
577 hours to synchronize and arrest cells in metaphase. MEFs were subsequently shaken off and
578 resuspended in hypotonic solution (56 mM KCl) for 60 min. The harvested cells were then
579 gradually fixed in 3:1 Methanol:Glacial Acetic Acid under constant agitation. Cells were pelleted
580 by centrifugation, the fixative decanted off, and re-fixed for a total of 3-4 times. Following the
581 final fixation round cells were suspended in 1-2 mL of fixative and dropped onto slides from a
582 height of \sim 1 m. Slides were allowed to air dry for approximately 10 min and then stored at -20°C
583 until hybridization. Commercially synthesized oligos corresponding to the *M. pahari* sequence
584 was PCR amplified and fluorescently labelled via nick translation. The Genomic DNA sequence
585 of putative *M. pahari* centromere sequence, π -sat, is;

586 AAAACATGTATGTTCTTCCTGCTCTATTAGACGCATTGTAAAGATATCTGTAGAACAGCATAGGAATA
587 TGAGTGCACCTCTGAAACACATGGTATTCTAAGAATAATTCCCTCATGGCAGTCAGAGCACTAAGTA
588 CAACTATGTGCACTCATGATTCACTCTGTTTCTGAGTTTGCATGT and the primers used were
589 forward: 5'-AACATGTATGTTCTTCCTGCTCT-3', reverse: 5'-TGTACTTAGTGCTCTGAACTGCC-3'.

590 Briefly, 250-1000 ng of PCR-amplified DNA was combined with nick translation buffer (200 mM
591 Tris pH 7.5, 500 mM MgCl₂, 5mM Dithiothreitol, and 500 mg/mL Bovine Serum Albumin), 0.2 mM
592 dNTPs, 0.2 mM fluorescent nucleotides, 1 U DNase (Promega), and 1 U DNA Pol I (Thermo Fisher
593 Scientific). One of three fluorescent nucleotides was used for each satellite probe set:
594 Fluorescein-12-dUTP (Thermo Fisher Scientific), ChromaTide Texas Red-12-dUTP (Thermo Fisher
595 Scientific/Invitrogen), and Alexa Fluor 647-aha-dUTP (Thermo Fisher Scientific/Invitrogen). The
596 reaction mixture was incubated at 14.5 °C for 90 min, and then terminated by addition of 10 mM

597 EDTA. Probes ranged from 50-200 bp in size, as assessed by gel electrophoresis. Probes were
598 used in FISH reactions on MEF metaphase cell spreads. Probes were denatured in hybridization
599 buffer (50% formamide, 10% Dextran Sulfate, 2x saline-sodium citrate [SSC], and mouse Cot-
600 1 DNA) at 72°C for 10 min and then allowed to re-anneal at 37°C until slides were ready for
601 hybridization. Slides were dehydrated in a sequential ethanol series (70%, 90%, and 100%; each
602 5 min) and dried at 42°C. Slides were then denatured in 70% formamide/2x SSC at 72°C for 3 min,
603 and immediately quenched in ice cold 70% ethanol for 5 min. Slides were subjected to a second
604 ethanol dehydration series (90% and 100%; each 5 min) and air dried. The probe hybridization
605 solution was then applied to the denatured slide. The hybridized region was then cover-slipped
606 and sealed with rubber cement. Hybridization reactions were allowed to occur overnight in a
607 humidified chamber at 37°C. After gently removing the rubber cement and soaking off coverslips,
608 slides were washed 2 times in 50% formamide/2x SSC followed by an additional two washes in
609 2x SSC for 5 min at room temperature. Slides were counterstained in 80 ng/mL DAPI (Thermo
610 Fisher Scientific/Invitrogen) for 10 min and air dried at room temperature. Lastly, slides were
611 mounted with ProLong Gold AntiFade (Thermo Fisher Scientific/Invitrogen) and stored at -20°C
612 until imaging. FISH reactions were imaged at 63x magnification on a Leica DM6B upright
613 fluorescent microscope equipped with fluorescent filters (Leica model numbers: 11504203,
614 11504207, 11504164), LED illumination, and a cooled monochrome Leica DFC7000 GT 2.8
615 megapixel digital camera. Images were captured using LAS X (Version 3.7) at a resolution of 1920
616 x 1440 pixels.

617 FISH of π -sat^B and the π -sat^B CENP-B box was performed as described earlier (53) with
618 some modifications. For FISH on metaphase spreads, *M. pahari* lung fibroblast cells were treated
619 with 50 μ M STLC (Sigma-Aldrich) for 2-4 hours to arrest cells during mitosis. Mitotic cells were
620 blown off using a transfer pipette and swollen in a hypotonic buffer consisting of a of 75 mM KCl
621 for 15 min. 3×10^4 cells were cytospun in an EZ Single Cytofunnel in a Shandon Cytospin 4 onto an
622 ethanol-washed positively charged glass slide and allowed to adhere for 1 min before
623 permeabilizing with KCM buffer for 15 min. For interphase FISH, cells were seeded on a positively
624 charged glass slide before permeabilizing with KCM buffer for 15 min. Slides were washed three
625 times in KCM for 5 min at RT. Slides were fixed in 4% formaldehyde in PBS, before washing three
626 times in dH₂O for 1 min each. Slides were incubated with 5 μ g/mL RNase A in 2x SSC at 37°C for
627 5 min. Cells were subjected to an ethanol series to dehydrate the cells and then denatured in
628 70% formamide/2x SSC at 77°C for 2.5 min. Cells were dehydrated with an ethanol series.

629 Biotinylated π -sat^B DNA probe was generated by PCR using the template sequence
630 TTTGAATCTAGATTGTTAGCTAGAACATACCATGTTCCGGAAC TGCACTCATATTGATCTGCTTTACT
631 ACAGAAATCTCTACAAAGCGTCTAATAGAGCAGGAAGAAAAATACCGTTTACACGAAAAACTCTTGA
632 AATACAGAGTGAATCCTGAGTGCAGATACTTGACTTAGTGCCTGAACAAAGAATTGAGGAATGTAAAG
633 GATCCTAT and the primers used were forward: 5'-GTTTAGCTTAGAACATACCATGTTT-3' and reverse:
634 5'-TTCCTCAATTCTGTTCAGAG-3' with Biotin-11 dUTP (ThermoFischer Scientific; AM8450),
635 purified with a G-50 spin column (Illustra), and ethanol-precipitated with salmon sperm DNA and
636 Cot-1 DNA. Precipitated π -sat^B was suspended in 50% formamide/10% dextran sulfate in 2x SSC
637 and denatured at 77°C for 5-10 min before being placed at 37 °C for at least 20 min. 100 ng DNA
638 probe was incubated with the cells on a glass slide at 37°C overnight in a dark, humidified
639 chamber. The CENP-B box probe was ordered from PNABio with a Cy3 fluorophore conjugated
640 to the sequence TTTCGTGTAAAACGGGT. PNA probe was prepared as described previously
641 (https://www.pnabio.com/pdf/FISH_protocol_PNABio.pdf). 50 μ M of PNA probe was
642 resuspended in formamide, heated to 55°C for 5 min and stored in aliquots at -80°C. After
643 thawing, probe was diluted 1:100 in 10 mM Tris-HCl pH 7.2, 70% formamide, 10 mM malic acid,
644 15 mM NaCl, and 0.5% blocking reagent (Roche 11096176001). Probe was denatured at 77°C for
645 5-10 min before being placed at 37°C for at least 20 min. 10 μ L of probe was incubated with the
646 cells on a glass slide at 37°C overnight in a dark, humidified chamber. The next day, slides were
647 washed two times with 50% formamide in 2x SSC for 5 min at 45°C. Next, slides were washed two
648 times with 0.1x SSC for 5 min at 45°C. Slides were blocked with 2.5% milk in 4x SSC with 0.1
649 Tween-20 for 10 min. For the π -sat^B FISH, Cells were incubated with NeutrAvidin-FITC
650 (ThermoFisher Scientific; 31006) diluted to 25 μ g/mL in 2.5% milk with 4x SSC and 0.1% Tween-
651 20 for 1 hour at 37°C in a dark, humidified chamber. Cells were washed three times with 4x SSC
652 and 0.1% Tween 20 at 45°C, DAPI-stained, and mounted on a glass coverslip with Vectashield
653 (Vector Labs).

654

655 ***Pulsed-Field gel electrophoresis and Southern blot***

656 Pahari mouse genomic DNA was prepared in agarose plugs and digested with BstXI and
657 HpaI enzymes by the manufacturer recommendation. The digested DNA was separated with the
658 CHEF Mapper system (Bio-Rad; Run conditions for 5-1000 kbp range: 0.5x TBE, 1% pulse field
659 certified agarose, 14°C, auto program, 16 hours run; Run conditions for 500-6000 kbp range: 1x
660 TAE, 1% pulse field certified agarose, 14°C, 2 V/cm, 106° included angle, 5-40 min field switching

661 with linear ramp, 92 hours run), transferred to a membrane (Amersham Hybond-N⁺), and blot-
662 hybridized with a 30 bp probe specific to the *M. pahari* centromeres (5'-
663 TTCTGTAAAACGGGTATTTCTTCCTGC-3'). To label the probe, 5' and 3' adapters below primers
664 were added. The probe was labeled with ³²P by PCR-amplifying a synthetic DNA template (5'-
665 TTTGTGGAAGTGGACATTCTCGTGTAAAACGGGTATTTCTTCCTGCTAAAAATAGACAGAACATT-
666 3') with primers forward: 5'-TTTGTGGAAGTGGACATTTC-3' and reverse: 5'-
667 AATGCTTCTGTCTATTTTA-3'. The blot was incubated for 2 hours at 65°C for pre-hybridization in
668 Church's buffer (0.5 M Na-phosphate buffer containing 7% SDS and 100 µg/mL of unlabeled
669 salmon sperm carrier DNA). The labeled probe was heat denatured in a boiling water bath for 5
670 min and snap-cooled on ice. The probe was added to the hybridization Church's buffer and
671 allowed to hybridize for 48 hours at 65°C. The blot was washed twice in 2× SSC (300 mM NaCl,
672 30 mM sodium citrate, pH 7.0), 0.05% SDS for 10 min at room temperature, and four times in 2×
673 SSC, 0.05% SDS for 5 min each at 60°C. The blot was exposed to X-ray film for 1-16 hours at -
674 80°C.

675

676 ***Immunofluorescence and microscopy for immortalized mouse lung fibroblast cells***

677 For a co-seed experiment involving CENP-A and CENP-B immunofluorescence, *M. pahari*
678 and *M. musculus* immortalized lung fibroblast cells were co-plated in 1:1 ratio. For experiments
679 involving H3K9Me3 immunofluorescence mouse lung fibroblast cells were fixed in 4%
680 formaldehyde for 10 min at room temperature and quenched with 100 mM Tris (pH 7.5) for 5
681 min, followed by permeabilization with 0.5% Triton X-100 for 5 min at room temperature. All
682 coverslips were then blocked in PBS supplemented with 2% fetal bovine serum, 2% bovine serum
683 albumin, and 0.1% Tween before antibody incubation. The following primary antibodies were
684 used: mouse mAb anti-mouse CENP-B (1:200, Santa Cruz Laboratories, (F4) sc-376283), rabbit
685 pAb anti-mouse CENP-A (1:500, 0.535 µg/mL; custom-made by Covance and affinity-purified in-
686 house), rabbit pAb anti-human H3K9Me3 (1:500, Abcam ChIP grade ab-8898), rabbit pAb anti-
687 human MCAK a gift from D. Compton (Dartmouth), and rabbit pAb anti-mouse Hec1^{Ndc80} antibody
688 (54). Secondary antibodies conjugated to fluorophores were used: FITC Goat anti-Mouse (1:200,
689 Jackson ImmunoResearch Laboratories # 115-095-146), Cy3 Goat anti-Rabbit (1:200, Jackson
690 ImmunoResearch Laboratories #111-165-144). Samples were stained with DAPI before mounting
691 with VectaShield medium (Vector Laboratories). For metaphase chromosome spread, cells were
692 treated with 50 µM STLC for 4 hours to arrest the cells during mitosis. Mitotic cells were blown

693 off using a transfer pipette and swollen in a hypotonic buffer consisting of a 1:1:1 ratio of 75 mM
694 KCl, 0.8% NaCitrate, 3 mM CaCl₂, and 1.5 mM MgCl₂ for 15 min at room temperature. 5 x 10⁴ cells
695 were cytospun onto a ethanol washed Superfrost Plus glass slide at 1500 rpm for 5 min and
696 allowed to adhere for 2 min before fixing with 4% formaldehyde. Cells were permeabilized with
697 0.5% Triton X-100 for 15 min at room temperature followed by immunostaining. Images were
698 captured at room temperature on an inverted fluorescence microscope (DFC9000 GT; Leica)
699 equipped with a charge-coupled device camera (ORCA AG; Hamamatsu Photonics) and a 100x,
700 1.4 NA oil immersion objective. Images were collected as 0.2 μm Z-sections using identical
701 acquisition conditions and Z series were deconvolved using LAS-X software (Leica). The
702 fluorescence intensity was measured from deconvolved and maximum-projected images by
703 ImageJ using 8 x 8 for H3K9Me3, 1.3 x 1.3 for MCAK, and 2.4 x 2.4 pixel box for Hec1^{Ndc80} using
704 CENP-B as a refrence channel. The local background intensity was substracted from the measured
705 fluorescence intensity. A minimum of 300 centromeres with low abundance of CENP-B and a
706 minimum of 40 centromeres with high abundance of CENP-B were counted from at least two
707 independent experiments. The mean ratio ± SEM is reported. For micronuclei experiment, *M.*
708 *pahari* cells were arrested with nocodazole for 6 hours and then released for 16 hours. Cells were
709 fixed with 4% formaldehyde for 10 min at room temperature and immunofluorescence was
710 performed as described above.

711

712 **Acknowledgements**

713 We thank our UPenn colleagues G. Birchak and K. McCannell for discussion, and L.
714 Chmátl for isolating the *M. pahari* primary lung fibroblast cells. We also thank B. Sullivan (Duke)
715 for sharing the protocol for mouse CENP-A antibody production, B. Johnson (Upenn) for providing
716 the SV40 large T antigen plasmid, and D. Compton (Dartmouth) for providing the human MCAK
717 antibody.

718

719 **Funding**

720 This work was supported by NIH grants GM130302 (B.E.B.), GM108360 (J.D.M.),
721 K99 GM147352 (G.A.L.), GM133415 (B.L.D.), F31 CA268727 (U.P.A.), and a Basser Center for
722 BRCA Early Career Award (N.P.).

723

724

725 **Author contributions**

726 C.W.G., N.P., J.M.D.-M., U.P.A., M.A.Li., M.A.La., G.A.L., B.L.D., and B.E.B. designed
727 experiments. C.W.G., N.P., J.M.D.-M., U.P.A., M.A.Li., and G.A.L. performed experiments and
728 analyzed data. J.M., P.L., and M.A.La. provided animal reagents. C.W.G., N.P., and B.E.B. wrote
729 the paper. All authors edited the manuscript. B.E.B. directed the research.

730

731 **Competing interests**

732 The authors declare that they have no competing interests.

733

734 **Data and materials availability**

735 All sequencing data will be made publicly available at the time of publication on GenBank
736 (centromere sequence assemblies) and SRA (raw sequencing files from Illumina, PACBio HiFi, and
737 ONT). All data has been uploaded to PRJNA966193. All other data needed to evaluate the
738 conclusions in the paper are present in the paper. The materials used in this study are
739 available from commercial sources or from the corresponding author on reasonable request.

740

741

742

743 **References**

744 1. K. Kixmoeller, P. K. Allu, B. E. Black, The centromere comes into focus: from CENP-A
745 nucleosomes to kinetochore connections with the spindle. *Open Biol.* **10**, 200051 (2020).

746 2. M. Dumont, D. Fachinetti, DNA sequences in centromere formation and function. *Prog Mol*
747 *Subcell Biol.* **56**, 305–336 (2017).

748 3. M. A. Lampson, B. E. Black, Cellular and molecular mechanisms of centromere drive. *Cold*
749 *Spring Harb Symp Quant Biol.* **82**, 249–257 (2017).

750 4. A. Iwata-Otsubo, J. M. Dawicki-McKenna, T. Akera, S. J. Falk, L. Chmátal, K. Yang, B. A. Sullivan,
751 R. M. Schultz, M. A. Lampson, B. E. Black, Expanded satellite repeats amplify a discrete CENP-
752 A nucleosome assembly site on chromosomes that drive in female meiosis. *Curr Biol.* **27**,
753 2365-2373.e8 (2017).

754 5. S. Henikoff, K. Ahmad, H. S. Malik, The centromere paradox: stable inheritance with rapidly
755 evolving DNA. *Science.* **293**, 1098–1102 (2001).

756 6. D. Dudka, M. A. Lampson, Centromere drive: model systems and experimental progress.
757 *Chromosome Res.* **30**, 187–203 (2022).

758 7. T. Akera, L. Chmátal, E. Trimm, K. Yang, C. Aonbangkhen, D. M. Chenoweth, C. Janke, R. M.
759 Schultz, M. A. Lampson, Spindle asymmetry drives non-Mendelian chromosome
760 segregation. *Science.* **358**, 668–672 (2017).

761 8. T. Akera, E. Trimm, M. A. Lampson, Molecular strategies of meiotic cheating by selfish
762 centromeres. *Cell.* **178**, 1132-1144.e10 (2019).

763 9. E. V. Linardopoulou, E. M. Williams, Y. Fan, C. Friedman, J. M. Young, B. J. Trask, Human
764 subtelomeres are hot spots of interchromosomal recombination and segmental duplication.
765 *Nature.* **437**, 94–100 (2005).

766 10. S. Nurk, S. Koren, A. Rhie, M. Rautiainen, A. V. Bzikadze, A. Mikheenko, M. R. Vollger, N.
767 Altemose, L. Uralsky, A. Gershman, S. Aganezov, S. J. Hoyt, M. Diekhans, G. A. Logsdon, M.
768 Alonge, S. E. Antonarakis, M. Borchers, G. G. Bouffard, S. Y. Brooks, G. V. Caldas, N.-C. Chen,
769 H. Cheng, C.-S. Chin, W. Chow, L. G. de Lima, P. C. Dishuck, R. Durbin, T. Dvorkina, I. T. Fiddes,
770 G. Formenti, R. S. Fulton, A. Fungtammasan, E. Garrison, P. G. S. Grady, T. A. Graves-Lindsay,
771 I. M. Hall, N. F. Hansen, G. A. Hartley, M. Haukness, K. Howe, M. W. Hunkapiller, C. Jain, M.
772 Jain, E. D. Jarvis, P. Kerpedjiev, M. Kirsche, M. Kolmogorov, J. Korlach, M. Kremitzki, H. Li, V.
773 V. Maduro, T. Marschall, A. M. McCartney, J. McDaniel, D. E. Miller, J. C. Mullikin, E. W.

774 Myers, N. D. Olson, B. Paten, P. Peluso, P. A. Pevzner, D. Porubsky, T. Potapova, E. I. Rogaev,
775 J. A. Rosenfeld, S. L. Salzberg, V. A. Schneider, F. J. Sedlazeck, K. Shafin, C. J. Shew, A.
776 Shumate, Y. Sims, A. F. A. Smit, D. C. Soto, I. Sović, J. M. Storer, A. Streets, B. A. Sullivan, F.
777 Thibaud-Nissen, J. Torrance, J. Wagner, B. P. Walenz, A. Wenger, J. M. D. Wood, C. Xiao, S.
778 M. Yan, A. C. Young, S. Zarate, U. Surti, R. C. McCoy, M. Y. Dennis, I. A. Alexandrov, J. L.
779 Gerton, R. J. O'Neill, W. Timp, J. M. Zook, M. C. Schatz, E. E. Eichler, K. H. Miga, A. M.
780 Phillippy, The complete sequence of a human genome. *Science*. **376**, 44–53 (2022).

781 11. M. Zetka, D. Paouneskou, V. Jantsch, The nuclear envelope, a meiotic jack-of-all-trades. *Curr
782 Opin Cell Biol.* **64**, 34–42 (2020).

783 12. R. K. Dawe, E. G. Lowry, J. I. Gent, M. C. Stitzer, K. W. Swentowsky, D. M. Higgins, J. Ross-
784 Ibarra, J. G. Wallace, L. B. Kanizay, M. Alabady, W. Qiu, K.-F. Tseng, N. Wang, Z. Gao, J. A.
785 Birchler, A. E. Harkess, A. L. Hodges, E. N. Hiatt, A Kinesin-14 motor activates
786 neocentromeres to promote meiotic drive in Maize. *Cell*. **173**, 839-850.e18 (2018).

787 13. T. A. Kato Yamakake, Cytological studies of maize [Zea mays L.] and teosinte [Zea mexicana
788 Schrader Kuntze] in relation to their origin and evolution (*Massachusetts Agricultural
789 Experiment Station, Amherst, Mass., 1976*), Research bulletin (*Massachusetts Agricultural
790 Experiment Station*).

791 14. M. M. Rhoades, H. Vilkomerson, On the anaphase movement of chromosomes. *Proc Natl
792 Acad Sci U S A*. **28**, 433–436 (1942).

793 15. C. M. Wade, E. Giulotto, S. Sigurdsson, M. Zoli, S. Gnerre, F. Imsland, T. L. Lear, D. L. Adelson,
794 E. Bailey, R. R. Bellone, H. Blöcker, O. Distl, R. C. Edgar, M. Garber, T. Leeb, E. Mauceli, J. N.
795 MacLeod, M. C. T. Penedo, J. M. Raison, T. Sharpe, J. Vogel, L. Andersson, D. F. Antczak, T.
796 Biagi, M. M. Binns, B. P. Chowdhary, S. J. Coleman, G. Della Valle, S. Fryc, G. Guérin, T.
797 Hasegawa, E. W. Hill, J. Jurka, A. Kiiilainen, G. Lindgren, J. Liu, E. Magnani, J. R. Mickelson,
798 J. Murray, S. G. Nergadze, R. Onofrio, S. Pedroni, M. F. Piras, T. Raudsepp, M. Rocchi, K. H.
799 Røed, O. A. Ryder, S. Searle, L. Skow, J. E. Swinburne, A. C. Syvänen, T. Tozaki, S. J. Valberg,
800 M. Vaudin, J. R. White, M. C. Zody, Broad Institute Genome Sequencing Platform, Broad
801 Institute Whole Genome Assembly Team, E. S. Lander, K. Lindblad-Toh, Genome sequence,
802 comparative analysis, and population genetics of the domestic horse. *Science*. **326**, 865–867
803 (2009).

804 16. D. P. Locke, L. W. Hillier, W. C. Warren, K. C. Worley, L. V. Nazareth, D. M. Muzny, S.-P. Yang,
805 Z. Wang, A. T. Chinwalla, P. Minx, M. Mitreva, L. Cook, K. D. Delehaunty, C. Fronick, H.

806 Schmidt, L. A. Fulton, R. S. Fulton, J. O. Nelson, V. Magrini, C. Pohl, T. A. Graves, C. Markovic,
807 A. Cree, H. H. Dinh, J. Hume, C. L. Kovar, G. R. Fowler, G. Lunter, S. Meader, A. Heger, C. P.
808 Ponting, T. Marques-Bonet, C. Alkan, L. Chen, Z. Cheng, J. M. Kidd, E. E. Eichler, S. White, S.
809 Searle, A. J. Vilella, Y. Chen, P. Fliceck, J. Ma, B. Raney, B. Suh, R. Burhans, J. Herrero, D.
810 Haussler, R. Faria, O. Fernando, F. Darré, D. Farré, E. Gazave, M. Oliva, A. Navarro, R.
811 Roberto, O. Capozzi, N. Archidiacono, G. Della Valle, S. Purgato, M. Rocchi, M. K. Konkel, J.
812 A. Walker, B. Ullmer, M. A. Batzer, A. F. A. Smit, R. Hubley, C. Casola, D. R. Schrider, M. W.
813 Hahn, V. Quesada, X. S. Puente, G. R. Ordoñez, C. López-Otín, T. Vinar, B. Brejova, A. Ratan,
814 R. S. Harris, W. Miller, C. Kosiol, H. A. Lawson, V. Taliwal, A. L. Martins, A. Siepel, A.
815 Roychoudhury, X. Ma, J. Degenhardt, C. D. Bustamante, R. N. Gutenkunst, T. Mailund, J. Y.
816 Dutheil, A. Hobolth, M. H. Schierup, O. A. Ryder, Y. Yoshinaga, P. J. de Jong, G. M. Weinstock,
817 J. Rogers, E. R. Mardis, R. A. Gibbs, R. K. Wilson, Comparative and demographic analysis of
818 orang-utan genomes. *Nature*. **469**, 529–533 (2011).

819 17. S. G. Nergadze, F. M. Piras, R. Gamba, M. Corbo, F. Cerutti, J. G. W. McCarter, E. Cappelletti,
820 F. Gozzo, R. M. Harman, D. F. Antczak, D. Miller, M. Scharfe, G. Pavesi, E. Raimondi, K. F.
821 Sullivan, E. Giulotto, Birth, evolution, and transmission of satellite-free mammalian
822 centromeric domains. *Genome Res.* **28**, 789–799 (2018).

823 18. M. Rocchi, R. Stanyon, N. Archidiacono, Evolutionary new centromeres in primates. *Prog Mol
824 Subcell Biol.* **48**, 103–152 (2009).

825 19. W.-H. Shang, T. Hori, A. Toyoda, J. Kato, K. Popendorf, Y. Sakakibara, A. Fujiyama, T.
826 Fukagawa, Chickens possess centromeres with both extended tandem repeats and short
827 non-tandem-repetitive sequences. *Genome Res.* **20**, 1219–1228 (2010).

828 20. T. Kumon, J. Ma, R. B. Akins, D. Stefanik, C. E. Nordgren, J. Kim, M. T. Levine, M. A. Lampson,
829 Parallel pathways for recruiting effector proteins determine centromere drive and
830 suppression. *Cell*. **184**, 4904-4918.e11 (2021).

831 21. H. Masumoto, H. Masukata, Y. Muro, N. Nozaki, T. Okazaki, A human centromere antigen
832 (CENP-B) interacts with a short specific sequence in alphoid DNA, a human centromeric
833 satellite. *J Cell Biol.* **109**, 1963–1973 (1989).

834 22. Y. Tanaka, O. Nureki, H. Kurumizaka, S. Fukai, S. Kawaguchi, M. Ikuta, J. Iwahara, T. Okazaki,
835 S. Yokoyama, Crystal structure of the CENP-B protein-DNA complex: the DNA-binding
836 domains of CENP-B induce kinks in the CENP-B box DNA. *EMBO J.* **20**, 6612–6618 (2001).

837 23. D. F. Pietras, K. L. Bennett, L. D. Siracusa, M. Woodworth-Gutai, V. M. Chapman, K. W. Gross,
838 C. Kane-Haas, N. D. Hastie, Construction of a small *Mus musculus* repetitive DNA library:
839 identification of a new satellite sequence in *Mus musculus*. *Nucleic Acids Res.* **11**, 6965–
840 6983 (1983).

841 24. H. F. Willard, J. S. Waye, Chromosome-specific subsets of human alpha satellite DNA: analysis
842 of sequence divergence within and between chromosomal subsets and evidence for an
843 ancestral pentameric repeat. *J Mol Evol.* **25**, 207–214 (1987).

844 25. D. Fachinetti, J. S. Han, M. A. McMahon, P. Ly, A. Abdullah, A. J. Wong, D. W. Cleveland, DNA
845 sequence-specific binding of CENP-B enhances the fidelity of human centromere function.
846 *Dev Cell.* **33**, 314–327 (2015).

847 26. M. Dumont, R. Gamba, P. Gestraud, S. Klaasen, J. T. Worrall, S. G. De Vries, V. Boudreau, C.
848 Salinas-Luypaert, P. S. Maddox, S. M. Lens, G. J. Kops, S. E. McClelland, K. H. Miga, D.
849 Fachinetti, Human chromosome-specific aneuploidy is influenced by DNA-dependent
850 centromeric features. *EMBO J.* **39**, e102924 (2020).

851 27. H. Nakagawa, J.-K. Lee, J. Hurwitz, R. C. Allshire, J.-I. Nakayama, S. I. S. Grewal, K. Tanaka, Y.
852 Murakami, Fission yeast CENP-B homologs nucleate centromeric heterochromatin by
853 promoting heterochromatin-specific histone tail modifications. *Genes Dev.* **16**, 1766–1778
854 (2002).

855 28. T. Okada, J. Ohzaki, M. Nakano, K. Yoda, W. R. Brinkley, V. Larionov, H. Masumoto, CENP-B
856 controls centromere formation depending on the chromatin context. *Cell.* **131**, 1287–1300
857 (2007).

858 29. K. Otake, J.-I. Ohzaki, N. Shono, K. Kugou, K. Okazaki, T. Nagase, H. Yamakawa, N. Kouprina,
859 V. Larionov, H. Kimura, W. C. Earnshaw, H. Masumoto, CENP-B creates alternative
860 epigenetic chromatin states permissive for CENP-A or heterochromatin assembly. *J Cell Sci.*
861 **133**, jcs243303 (2020).

862 30. A. K. Wong, J. B. Rattner, Sequence organization and cytological localization of the minor
863 satellite of mouse. *Nucleic Acids Res.* **16**, 11645–11661 (1988).

864 31. B. Dod, E. Mottez, E. Desmarais, F. Bonhomme, G. Roizés, Concerted evolution of light
865 satellite DNA in genus *Mus* implies amplification and homogenization of large blocks of
866 repeats. *Mol Biol Evol.* **6**, 478–491 (1989).

867 32. Y. Nishioka, Genome comparison in the genus *Mus*: a study with B1, MIF (mouse interspersed
868 fragment), centromeric, and Y-chromosomal repetitive sequences. *Cytogenet Cell Genet.*
869 **50**, 195–200 (1989).

870 33. U. P. Arora, C. Charlebois, R. A. Lawal, B. L. Dumont, Population and subspecies diversity at
871 mouse centromere satellites. *BMC Genomics*. **22**, 279 (2021).

872 34. D. Thybert, M. Roller, F. C. P. Navarro, I. Fiddes, I. Streeter, C. Feig, D. Martin-Galvez, M.
873 Kolmogorov, V. Janoušek, W. Akanni, B. Aken, S. Aldridge, V. Chakrapani, W. Chow, L. Clarke,
874 C. Cummins, A. Doran, M. Dunn, L. Goodstadt, K. Howe, M. Howell, A.-A. Josselin, R. C. Karn,
875 C. M. Laukaitis, L. Jingtao, F. Martin, M. Muffato, S. Nachtweide, M. A. Quail, C. Sisu, M.
876 Stanke, K. Stefflova, C. Van Oosterhout, F. Veyrunes, B. Ward, F. Yang, G. Yazdanifar, A.
877 Zadissa, D. J. Adams, A. Brazma, M. Gerstein, B. Paten, S. Pham, T. M. Keane, D. T. Odom, P.
878 Flíček, Repeat associated mechanisms of genome evolution and function revealed by the
879 *Mus caroli* and *Mus pahari* genomes. *Genome Res.* **28**, 448–459 (2018).

880 35. P. Novák, L. Ávila Robledillo, A. Koblížková, I. Vrbová, P. Neumann, J. Macas, TAREAN: a
881 computational tool for identification and characterization of satellite DNA from
882 unassembled short reads. *Nucleic Acids Res.* **45**, e111 (2017).

883 36. N. Altemose, G. A. Logsdon, A. V. Bzikadze, P. Sidhwani, S. A. Langley, G. V. Caldas, S. J. Hoyt,
884 L. Uralsky, F. D. Ryabov, C. J. Shew, M. E. G. Sauria, M. Borchers, A. Gershman, A. Mikheenko,
885 V. A. Shepelev, T. Dvorkina, O. Kunyavskaya, M. R. Vollger, A. Rhee, A. M. McCartney, M.
886 Asri, R. Lorig-Roach, K. Shafin, J. K. Lucas, S. Aganezov, D. Olson, L. G. de Lima, T. Potapova,
887 G. A. Hartley, M. Haukness, P. Kerpedjiev, F. Gusev, K. Tigli, S. Brooks, A. Young, S. Nurk, S.
888 Koren, S. R. Salama, B. Paten, E. I. Rogaev, A. Streets, G. H. Karpen, A. F. Dernburg, B. A.
889 Sullivan, A. F. Straight, T. J. Wheeler, J. L. Gerton, E. E. Eichler, A. M. Phillippy, W. Timp, M.
890 Y. Dennis, R. J. O'Neill, J. M. Zook, M. C. Schatz, P. A. Pevzner, M. Diekhans, C. H. Langley, I.
891 A. Alexandrov, K. H. Miga, Complete genomic and epigenetic maps of human centromeres.
892 *Science*. **376**, eabl4178 (2022).

893 37. G. A. Logsdon, M. R. Vollger, P. Hsieh, Y. Mao, M. A. Liskovskykh, S. Koren, S. Nurk, L. Mercuri,
894 P. C. Dishuck, A. Rhee, L. G. de Lima, T. Dvorkina, D. Porubsky, W. T. Harvey, A. Mikheenko,
895 A. V. Bzikadze, M. Kremitzki, T. A. Graves-Lindsay, C. Jain, K. Hoekzema, S. C. Murali, K. M.
896 Munson, C. Baker, M. Sorensen, A. M. Lewis, U. Surti, J. L. Gerton, V. Larionov, M. Ventura,
897 K. H. Miga, A. M. Phillippy, E. E. Eichler, The structure, function and evolution of a complete
898 human chromosome 8. *Nature*. **593**, 101–107 (2021).

899 38. K. H. Miga, S. Koren, A. Rhie, M. R. Vollger, A. Gershman, A. Bzikadze, S. Brooks, E. Howe, D.
900 Porubsky, G. A. Logsdon, V. A. Schneider, T. Potapova, J. Wood, W. Chow, J. Armstrong, J.
901 Fredrickson, E. Pak, K. Tigyi, M. Kremitzki, C. Markovic, V. Maduro, A. Dutra, G. G. Bouffard,
902 A. M. Chang, N. F. Hansen, A. B. Wilfert, F. Thibaud-Nissen, A. D. Schmitt, J.-M. Belton, S.
903 Selvaraj, M. Y. Dennis, D. C. Soto, R. Sahasrabudhe, G. Kaya, J. Quick, N. J. Loman, N. Holmes,
904 M. Loose, U. Surti, R. A. Risques, T. A. Graves Lindsay, R. Fulton, I. Hall, B. Paten, K. Howe,
905 W. Timp, A. Young, J. C. Mullikin, P. A. Pevzner, J. L. Gerton, B. A. Sullivan, E. E. Eichler, A. M.
906 Phillippy, Telomere-to-telomere assembly of a complete human X chromosome. *Nature*.
907 **585**, 79–84 (2020).

908 39. H. Cheng, E. D. Jarvis, O. Fedrigo, K.-P. Koepfli, L. Urban, N. J. Gemmell, H. Li, Haplotype-
909 resolved assembly of diploid genomes without parental data. *Nat Biotechnol*. **40**, 1332–
910 1335 (2022).

911 40. K. M. Godek, L. Kabeche, D. A. Compton, Regulation of kinetochore-microtubule attachments
912 through homeostatic control during mitosis. *Nat Rev Mol Cell Biol*. **16**, 57–64 (2015).

913 41. A. H. F. M. Peters, S. Kubicek, K. Mechtl, R. J. O'Sullivan, A. A. H. A. Derijck, L. Perez-Burgos,
914 A. Kohlmaier, S. Opravil, M. Tachibana, Y. Shinkai, J. H. A. Martens, T. Jenuwein, Partitioning
915 and plasticity of repressive histone methylation states in mammalian chromatin. *Mol Cell*.
916 **12**, 1577–1589 (2003).

917 42. O. J. Marshall, A. C. Chueh, L. H. Wong, K. H. A. Choo, Neocentromeres: new insights into
918 centromere structure, disease development, and karyotype evolution. *Am J Hum Genet*. **82**,
919 261–282 (2008).

920 43. G. Montefalcone, S. Tempesta, M. Rocchi, N. Archidiacono, Centromere repositioning.
921 *Genome Res*. **9**, 1184–1188 (1999).

922 44. F. Pardo-Manuel de Villena, C. Sapienza, Female meiosis drives karyotypic evolution in
923 mammals. *Genetics*. **159**, 1179–1189 (2001).

924 45. M. Rocchi, N. Archidiacono, W. Schempp, O. Capozzi, R. Stanyon, Centromere repositioning
925 in mammals. *Heredity*. **108**, 59–67 (2012).

926 46. M. Ventura, N. Archidiacono, M. Rocchi, Centromere emergence in evolution. *Genome Res*.
927 **11**, 595–599 (2001).

928 47. A. Seluanov, A. Vaidya, V. Gorbunova, Establishing primary adult fibroblast cultures from
929 rodents. *J Vis Exp*, 2033 (2010).

930 48. Y. Yu, J. C. Alwine, Human cytomegalovirus major immediate-early proteins and simian virus
931 40 large T antigen can inhibit apoptosis through activation of the phosphatidylinositide 3'-
932 OH kinase pathway and the cellular kinase Akt. *J Virol.* **76**, 3731–3738 (2002).

933 49. D. Hasson, T. Panchenko, K. J. Salimian, M. U. Salman, N. Sekulic, A. Alonso, P. E. Warburton,
934 B. E. Black, The octamer is the major form of CENP-A nucleosomes at human centromeres.
935 *Nat Struct Mol Biol.* **20**, 687–695 (2013).

936 50. H. Li, B. Handsaker, A. Wysoker, T. Fennell, J. Ruan, N. Homer, G. Marth, G. Abecasis, R.
937 Durbin, 1000 Genome project data processing subgroup, the sequence slignment/map
938 format and SAMtools. *Bioinformatics*. **25**, 2078–2079 (2009).

939 51. M. C. Frith, N. F. W. Saunders, B. Kobe, T. L. Bailey, Discovering sequence motifs with arbitrary
940 insertions and deletions. *PLoS Comput Biol.* **4**, e1000071 (2008).

941 52. M. Martin, Cutadapt removes adapter sequences from high-throughput sequencing reads.
942 *EMBnet.journal.* **17**, 10–12 (2011).

943 53. W. Bickmore, Fluorescence in situ hybridization analysis of chromosome and chromatin
944 structure. *Methods Enzymol.* **304**, 650–662 (1999).

945 54. E. Diaz-Rodríguez, R. Sotillo, J.-M. Schvartzman, R. Benezra, Hec1 overexpression
946 hyperactivates the mitotic checkpoint and induces tumor formation in vivo. *Proc Natl Acad
947 Sci U S A.* **105**, 16719–16724 (2008).

948

949

950 **Figure Legends**

951 Figure 1: CENP-B occupancy on centromere DNA does not impact CENP-A nucleosome phasing,
952 but does vary widely between and within mouse species.
953 A) Midpoint position of CENP-A ChIP H3K9Me3 or input reads (size 100–160 bp) from WT *M.*
954 *musculus* along the trimer minor satellite consensus sequence. Vertical lines indicate the 17-bp
955 CENP-B box. The major CENP-A nucleosome position (identified in the CENP-A ChIP samples) is
956 indicated by a horizontal black line above the respective midpoint values and schematized (inset)
957 for CENP-A ChIP with a triangle representing the dyad position. The same nucleosome position is
958 indicated in the H3K9Me3 and input samples. Numbers to the left of the positions indicate the
959 percentage of reads (mean \pm SEM; n = 3 independent experiments) where the midpoint spans
960 the 10 bp at the 3' end of the CENP-B box (yellow, labeled B). Horizontal gray lines indicate other
961 major nucleosome positions in the H3K9Me3 and input samples. B) Midpoint position of CENP-A
962 ChIP H3K9Me3 or input reads (size 100–160 bp) from CENP-B KO *M. musculus* along the trimer
963 minor satellite consensus sequence. C) Centromere satellites from *M. musculus*, *M. spretus*, and
964 *M. pahari*. D) CENP-B is highly conserved in mouse species, with 100% identical sequences in both
965 the DNA binding domain and the epitope targeted by the CENP-B antibody used in our study. E)
966 Immunofluorescence of CENP-A and CENP-B from lung fibroblast cells derived from *M. musculus*
967 (with their nuclei identified by strong DAPI-staining pericentromeres) or *M. pahari*. Bar, 10 μ m.
968

969 Figure 2: Identification of the most abundant form of centromere repeats in *M. pahari*: π -sat.
970 A) Two approaches to identify *M. pahari* centromeric repeats. B) Satellite sequences derived from
971 TAREAN analysis on input sequencing data. Satellite probability was calculated as described in
972 Methods. C) Representative image of *M. pahari* centromeric DNA labeled with FISH probe using
973 consensus sequence derived from k-mer approach. Insets: 7.9x magnification, Bar, 10 μ m. D)
974 Schematized representation of the 3 satellites identified by TAREAN analysis. E) Alignment of the
975 π -sat consensus sequence to minor sat consensus sequence. A dimer of π -sat was aligned to a
976 trimer of minor satellite and the first monomer of π -sat is shown. The end of first monomer of
977 minor satellite is marked with an asterisk. F) Histograms show distribution of reads from input,
978 CENP-A ChIP, or H3K9Me3 ChIP aligning to π -sat. G) Representative example of a π -sat containing
979 ONT long read that was divided into monomers. The percent identity of each monomer to π -sat
980 is plotted.

981

982 Figure 3: π -sat^B is highly homogenous, restricted to a single pair of chromosomes, and present in
983 long, contiguous blocks that lack generic π -sat.

984 A) Approach to identify CENP-B box containing satellite. B) Alignment of π -sat and π -sat^B. C)
985 Histograms show distribution of reads from input, CENP-A ChIP or H3K9Me3 ChIP aligning to π -
986 sat^B. D) Representative image of *M. pahari* centromeric DNA labeled with FISH probe using π -
987 sat^B consensus sequence. Insets: 2.5x magnification, Bar, 10 μ m. E) Logo representation of the
988 CENP-B box consensus of π -sat and π -sat^B. F) Plots of the percent identity of satellites along a
989 portion of representative ONT reads with (right) and without (left) CENP-B boxes to the π -sat
990 and π -sat^B consensus sequences.

991

992 Figure 4: Genomic assembly reveals the identity and nature of the centromere harboring π -sat^B.

993 A) The composition of the centromere of chromosome 11. The assembly consists of, in order, 8
994 kb of telomeric repeats, 6 Mbp of π -sat^B, 3.6 Mb of π -sat, 400 kb of π -sat^{tel}, followed by other
995 repetitive elements. The total number of CENP-B boxes (21,617) on this centromere is denoted.
996 The fraction of π -sat repeats containing a functional CENP-B box (NTTCGNNNNANNCGGGN) and
997 the frequency of telomeric repeats (TTAGGG) are shown. CENP-A ChIP-seq reads were aligned to
998 the chromosome 11 centromere assembly. A pairwise sequence identity heat map indicates that
999 the centromere consists of 6 Mbp of highly homogenous π -sat^B. B) Schematic of predicted
1000 restriction digest sites of chromosome 11 with BstXI and HpaI. Pulsed-field gel Southern blot of
1001 *M. pahari* DNA confirms the structure and organization of the chromosome 11 centromeric HOR
1002 array. For each gel, left corresponds to ethidium bromide (EtBr) staining and right, ³²P-labelled
1003 chromosome 11 π -sat^B specific probe. The left gel was run at conditions to separate DNA from
1004 0.6-5 Mb and the right gel was run at conditions to separate DNA from 5-1000 kb.

1005

1006 Figure 5: Evolutionarily older *M. pahari* centromeres harbor CENP-A nucleosomes near CENP-B
1007 boxes and π -sat^{tel}.

1008 A-D) The composition of a representative *M. pahari* centromeres. Each of the assembly consists
1009 of in order an array of telomeric repeats, an array of π -sat^{tel}, and an array of π -sat followed by
1010 various repetitive elements. The fraction of π -sat repeats containing a functional CENP-B box
1011 (NTTCGNNNNANNCGGGN) and the frequency of telomeric repeats (TTAGGG) are shown. CENP-
1012 A ChIP-seq reads were aligned to the assembly revealing that CENP-A is primarily present on π -

1013 sat^{tel}. A pairwise sequence identity heat map indicates the degree of homogeneity in centromeric
1014 DNA. E) The types of repeating units found at *M. pahari* centromeres.

1015
1016 Figure 6: Chromosome 11 harbors levels of both pro- and anti-microtubule binding proteins that
1017 are higher than on the other *M. pahari* centromeres.

1018 A) Immunofluorescence of H3K9Me3 from lung fibroblast cells derived from *M. pahari*. Insets:
1019 4.0x magnification, Bar, 10 μ m. Chromosomes are abbreviated as Chr in this figure. B)
1020 Quantification of H3K9Me3 from the experiment in panel A. The mean ratio (\pm SEM) is shown. n=
1021 314 for the centromeres with low abundance of CENP-B and n= 50 for the centromeres with high
1022 abundance of CENP-B, pooled from 2 independent experiments. C) Immunofluorescence of
1023 MCAK from lung fibroblast cells derived from *M. pahari*. Insets: 6.5x magnification, Bar, 10 μ m.
1024 D) Quantification of MCAK from the experiment in panel C. The mean ratio (\pm SEM) is shown. n=
1025 389 for the centromeres with low abundance of CENP-B and n= 45 for the centromeres with high
1026 abundance of CENP-B, pooled from 2 independent experiments. E) Immunofluorescence of
1027 Hec1^{Ndc80} from lung fibroblast cells derived from *M. pahari*. Insets: 5.1x magnification, Bar, 10
1028 μ m. F) Quantification of Hec1^{Ndc80} from the experiment in panel E. The mean ratio (\pm SEM) is
1029 shown. n= 324 for the centromeres with low abundance of CENP-B and n= 94 for the centromeres
1030 with high abundance of CENP-B, pooled from 3 independent experiments. G) Schematic for
1031 measuring micronuclei containing chromosome 11 or other chromosomes. H)
1032 Immunofluorescence of micronuclei with low and high abundance of CENP-B centromeres from
1033 lung fibroblast cells derived from *M. pahari*. Insets: 1.8x magnification, Bar, 10 μ m. I)
1034 Quantification of micronuclei from the experiment in panel H. Welch's t test showed no
1035 significant difference between the actual micronuclei frequency and the expected frequency if
1036 there is no bias. A grey line represents the expected frequency given no bias, n= 133 (- Noc) and
1037 n= 419 (+Noc), pooled from 4 independent experiments.

1038
1039 Figure 7: Divergent centromere DNA, molecular composition, and implications for mitotic
1040 chromosome segregation in *M. pahari*.

1041 A) Cartoon drawing summarizing the different types of *M. pahari* centromeres. The majority of
1042 *M. pahari* centromeres contain a low density of functional CENP-B boxes. Furthermore, these
1043 centromeres have two kinds of π -sat. First, the CENP-A containing region is a stretch of repeating
1044 units of π -sat that is short (~130 bp) or long (189 bp) and interspersed with telomeric repeats.

1045 This is adjacent to a longer stretch of repeating units of 189 bp π -sat. The second type of *M.*
1046 *pahari* centromere has a high density of CENP-B boxes and is only found on chromosome 11. This
1047 centromere consist of 6 Mbp of homogenous π -sat^B. The higher homogeneity of this centromeric
1048 DNA suggests that it is evolutionarily more recent relative to the other *M. pahari* centromeres.
1049 B) Model to understand different possible outcomes of centromere innovations during mitosis.
1050 The typical centromere has relatively low numbers of kinetochore attachments and relatively low
1051 amounts of microtubule destabilizer. These two factors balance each other allowing normal
1052 segregation during mitosis. If either pro- or anti-microtubule binding factors are increased in the
1053 absence of the other, there will be an imbalance resulting in incorrect segregation during mitosis.
1054 The chromosome 11 has higher levels of microtubule destabilizer and more microtubule
1055 attachments, but because both factors are increased together, the chromosomes can still
1056 undergo error-free mitosis.

1057

1058 **Supplementary Figure Legends:**

1059 Figure S1: π -sat sequence is almost identical to the top hit identified by the *k*-mer strategy
1060 Alignment of the satellites derived from the *k*-mer and TAREAN approach.

1061

1062 Figure S2: Functional CENP-B box is found at an pair of homologues containing π -sat^B.
1063 Representative image of *M. pahari* fibroblast cells labeled with CENP-B box and π -sat^B FISH
1064 probes. Insets: 4.6x magnification. Bar, 10 μ m.

1065

1066 Figure S3: Functional CENP-B boxes found at chromosome 11 differ from functional CENP-B boxes
1067 found on π -sat^{tel} on other centromeres.

1068 Alignment of functional CENP-B box from π -sat^B and π -sat^{tel}

1069

1070 Figure S4: Three additional *M. pahari* centromeres, all containing similar overall organization.
1071 A-C) The fraction of π -sat repeats containing a functional CENP-B box (NTTCGNNNNANNCGGGN)
1072 and the frequency of telomeric repeats (TTAGGG) are shown. CENP-A ChIP-seq reads were
1073 aligned to the assembly revealing that CENP-A is primarily present on π -sat^{tel}. A pairwise
1074 sequence identity heat map indicates the degree of homogeneity in centromeric DNA.

1075

1076

Figure 1

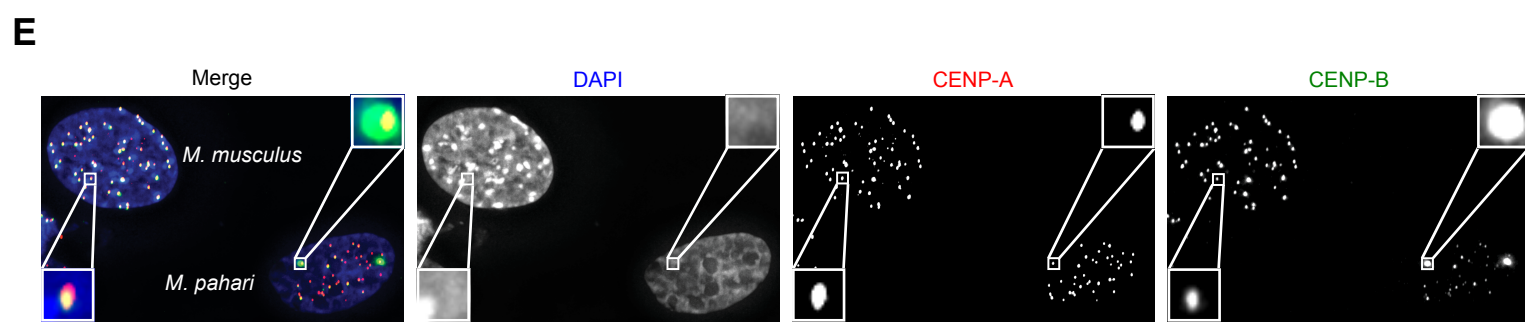
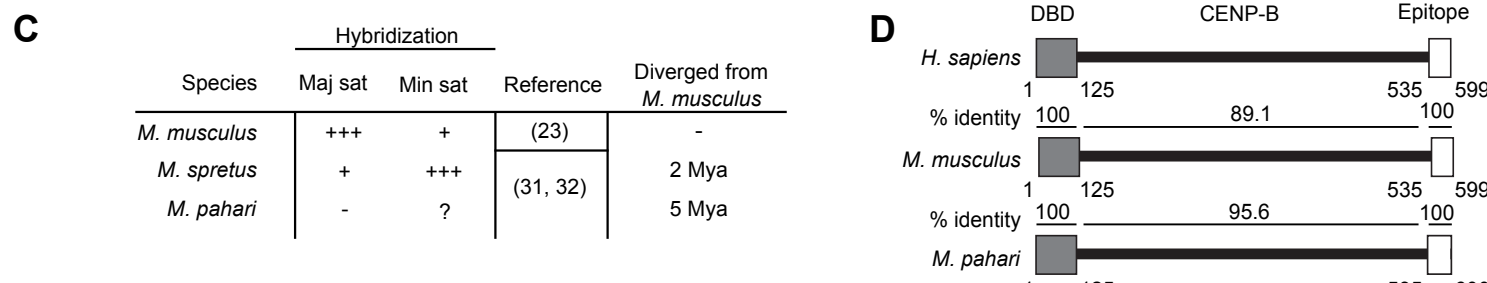
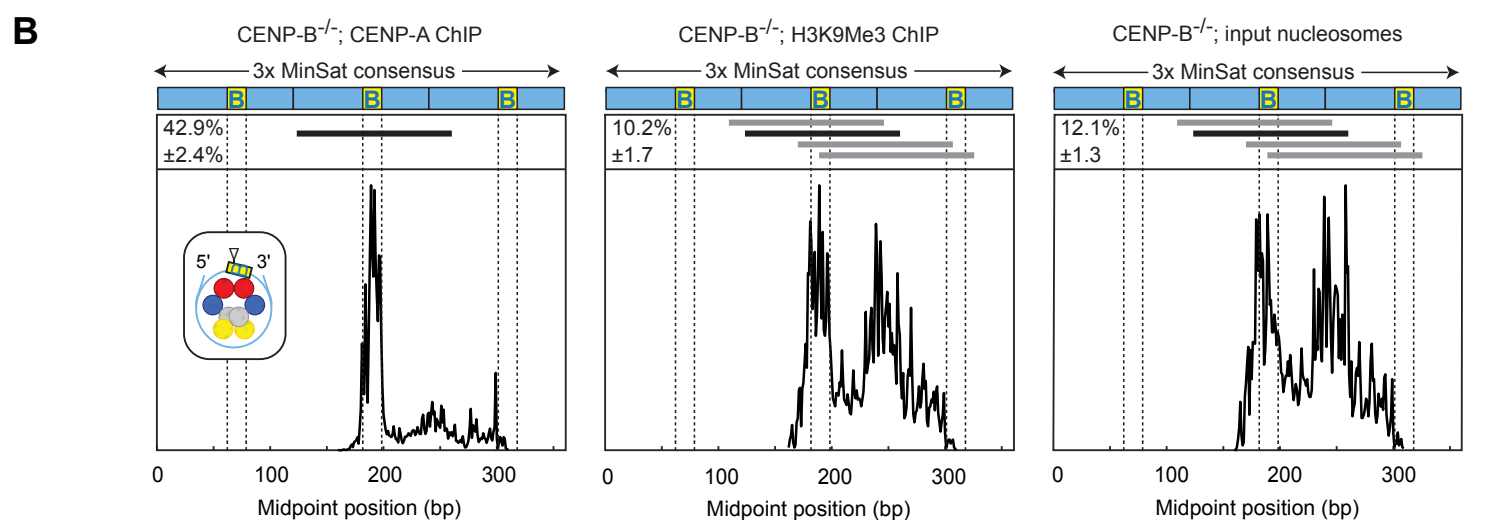
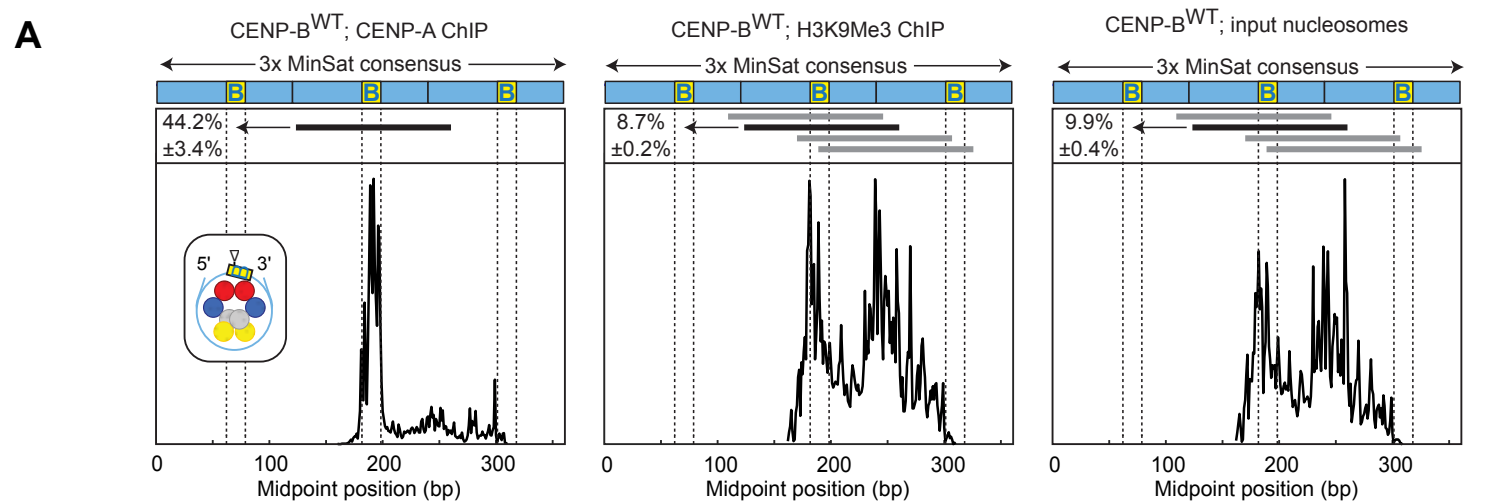


Figure 2

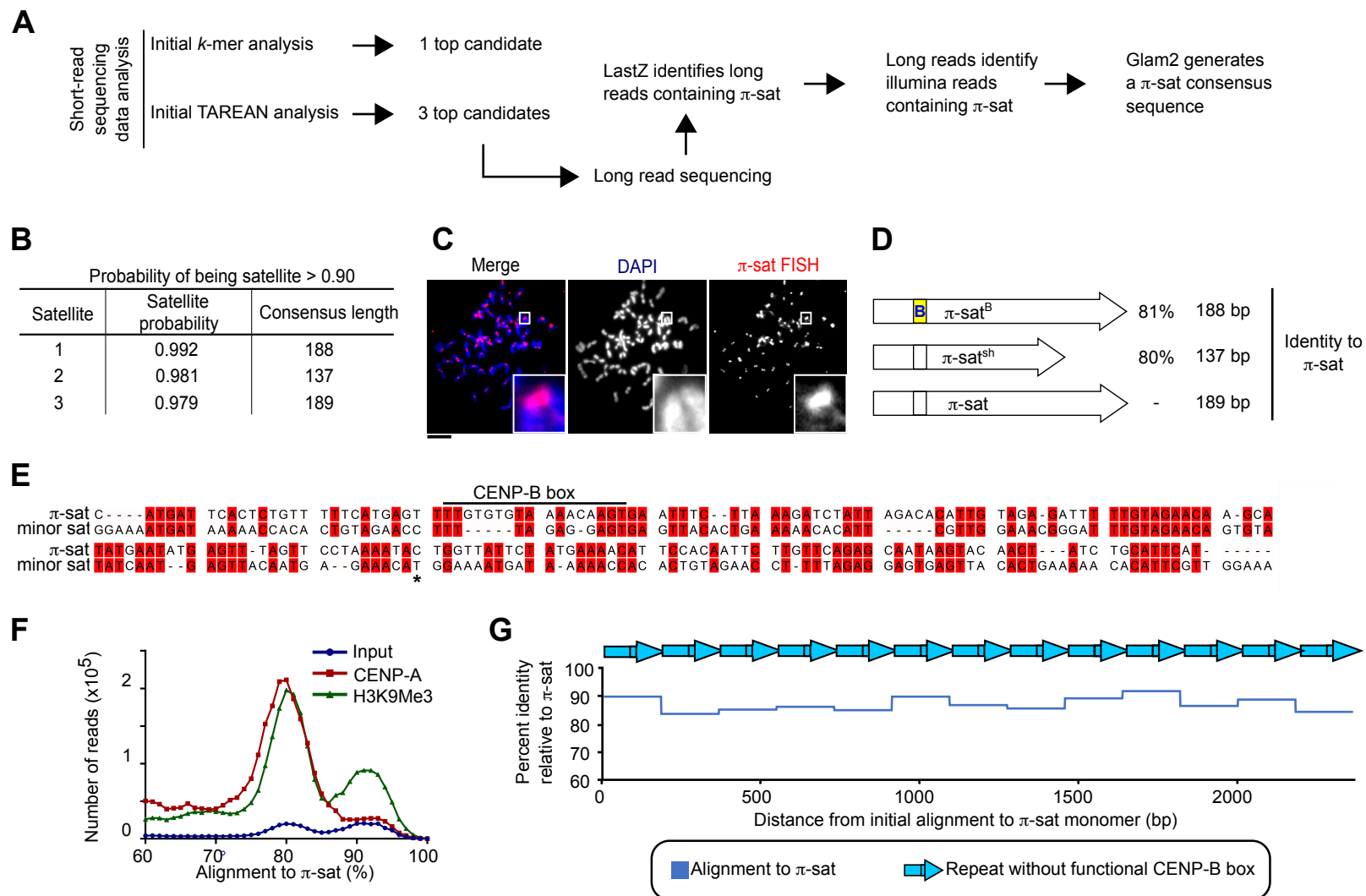


Figure 3

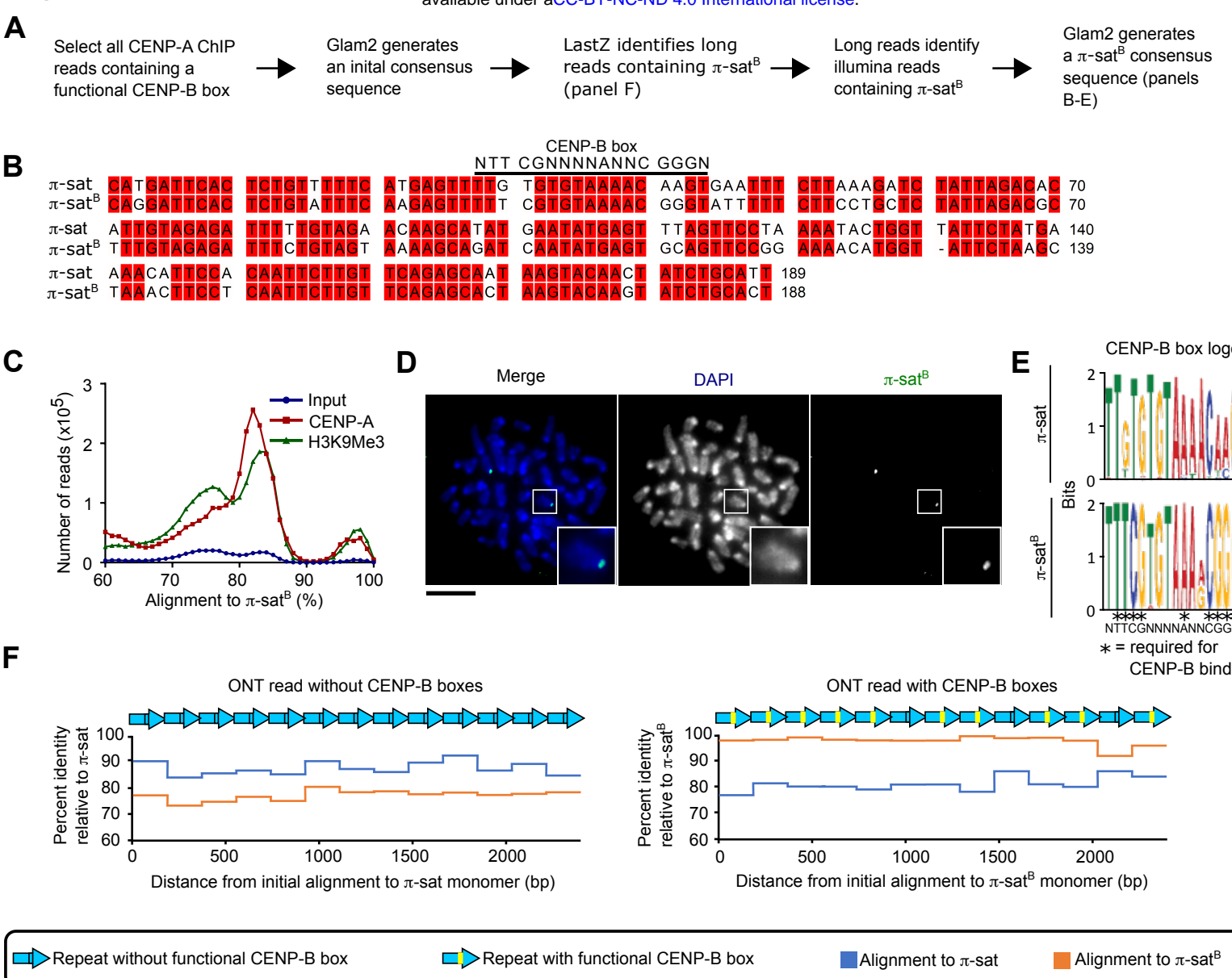


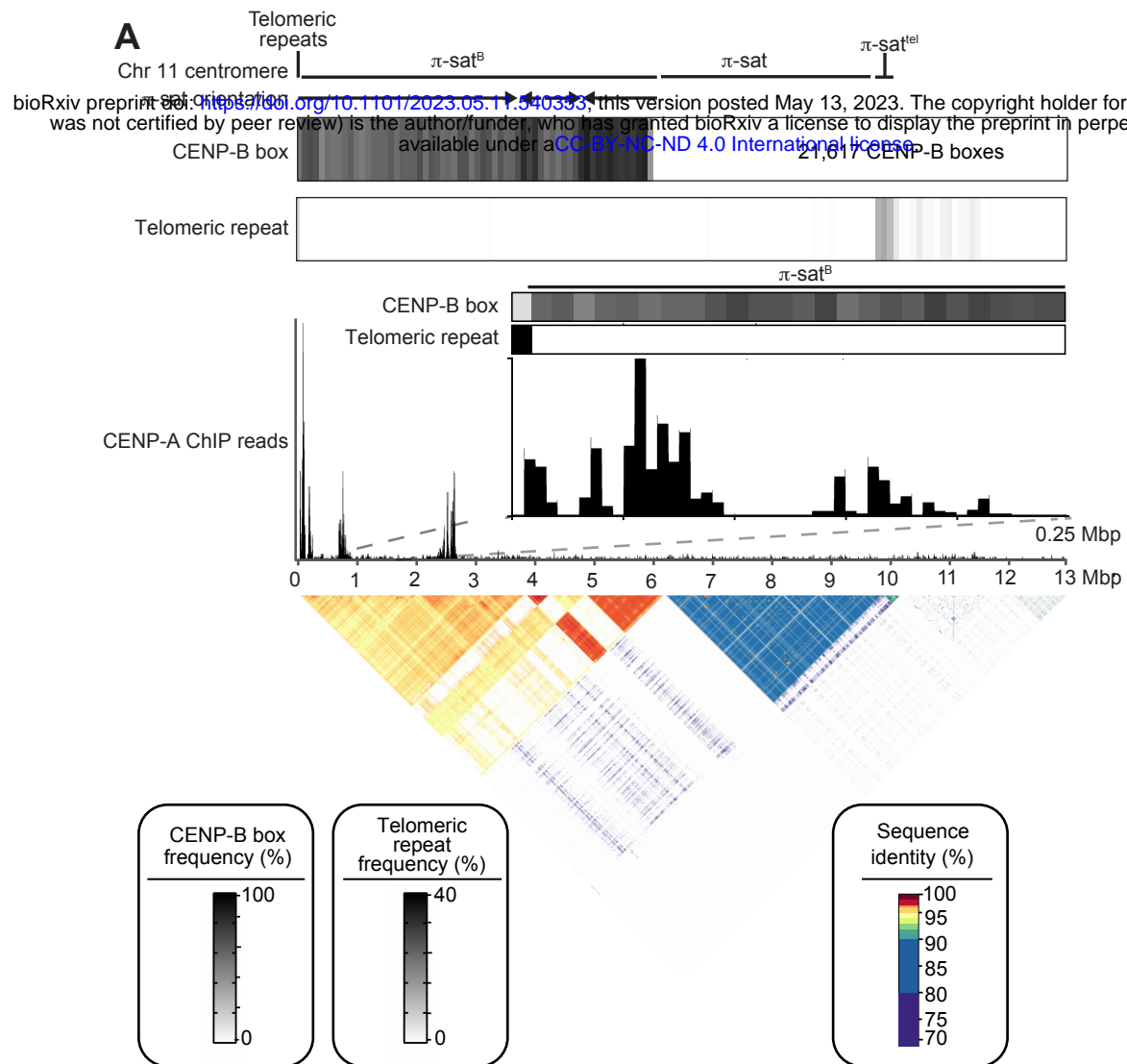
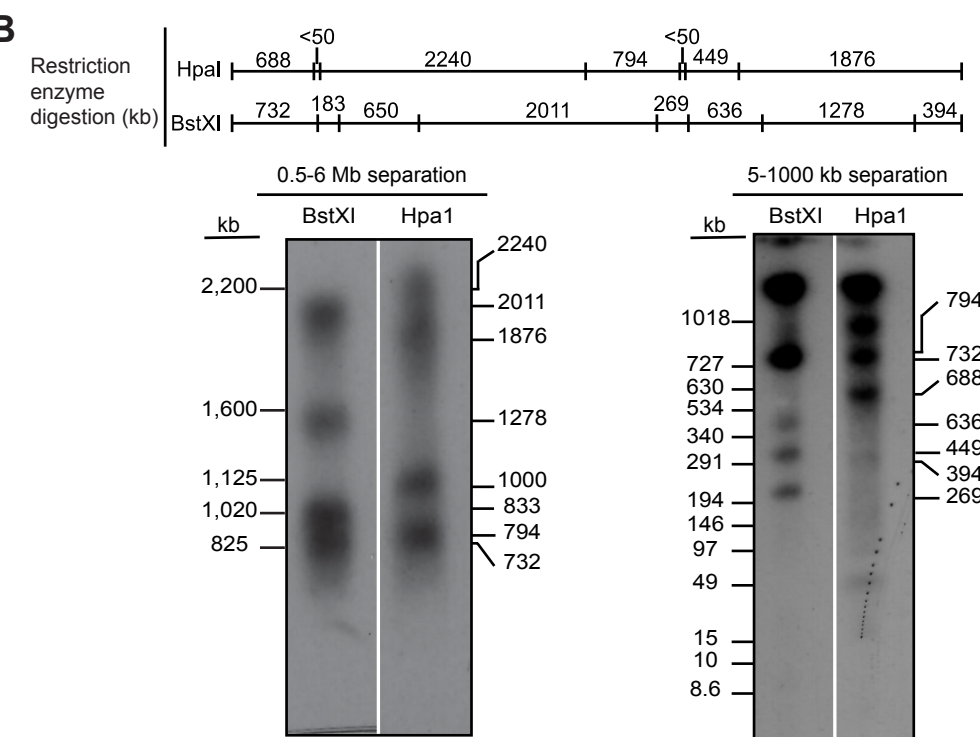
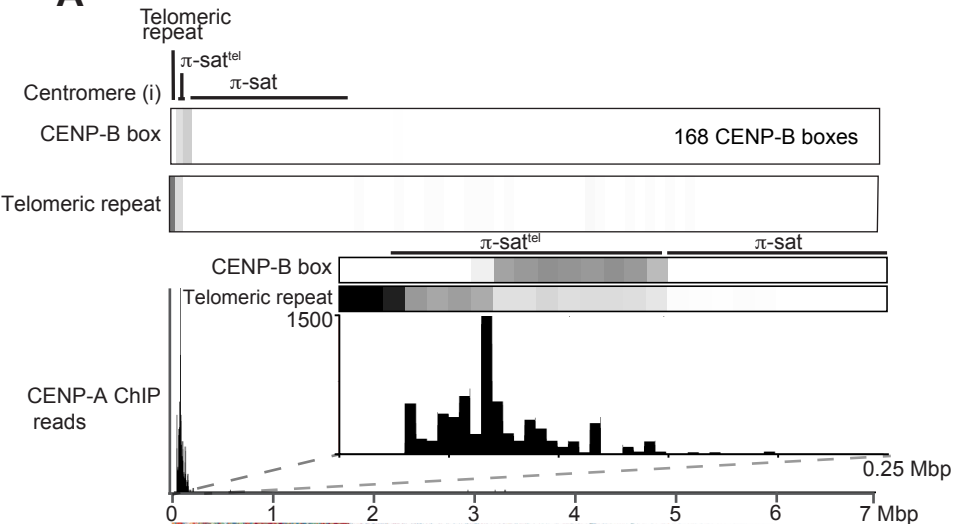
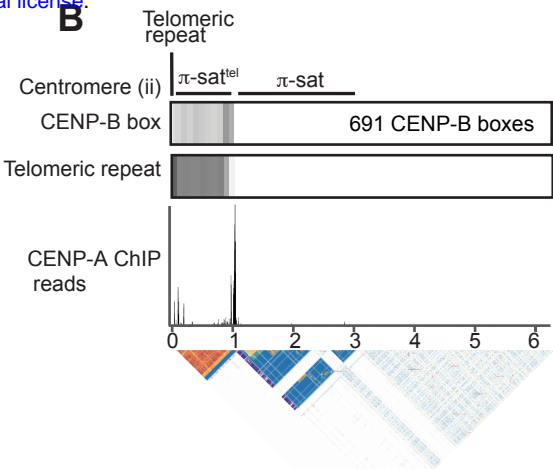
Figure 4**A****B**

Figure 5

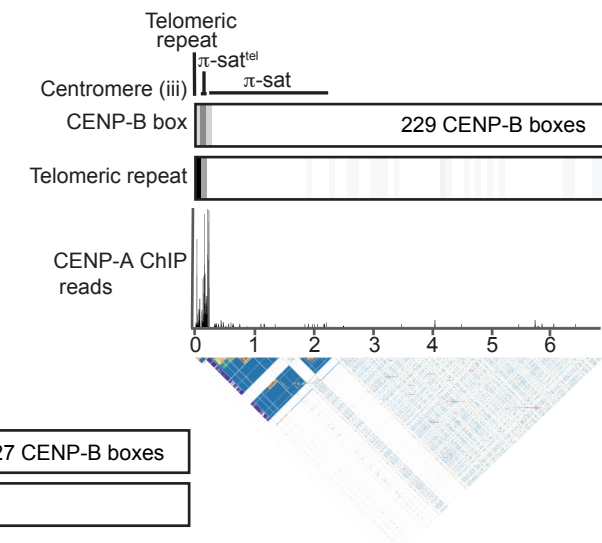
A



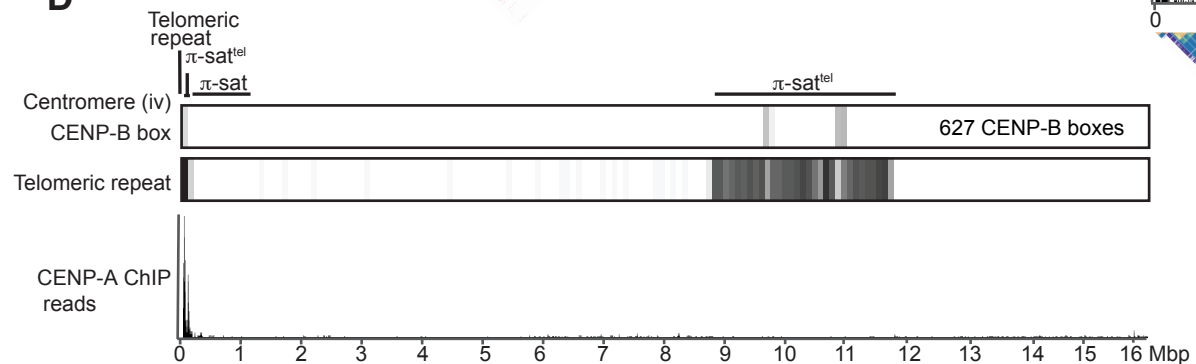
B



C



D



E

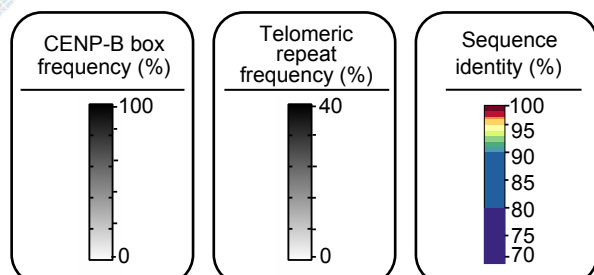
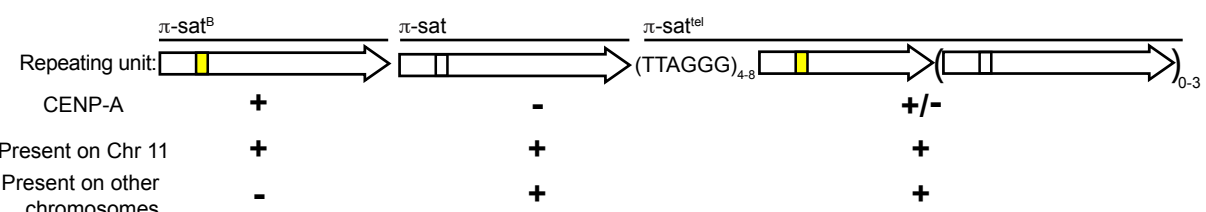
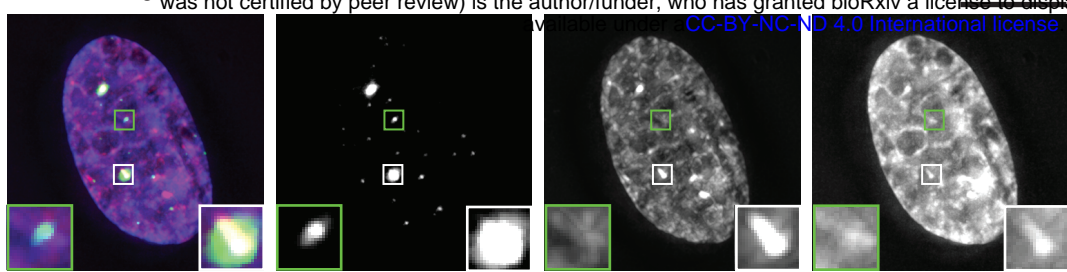


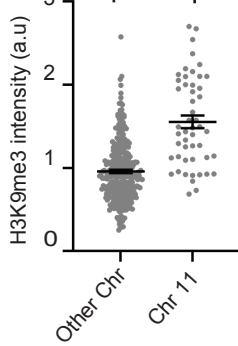
Figure 6

bioRxiv preprint doi: <https://doi.org/10.1101/2023.05.11.540353>; this version posted May 13, 2023. The copyright holder for this preprint (which was not certified by peer review) is the author/funder, who has granted bioRxiv a license to display the preprint in perpetuity. It is made available under a CC-BY-NC-ND 4.0 International license.

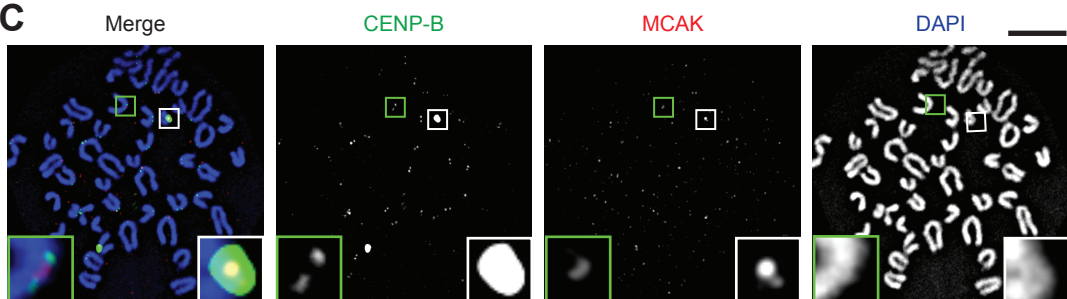
A



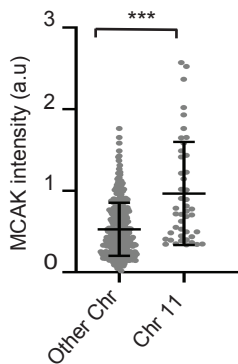
B



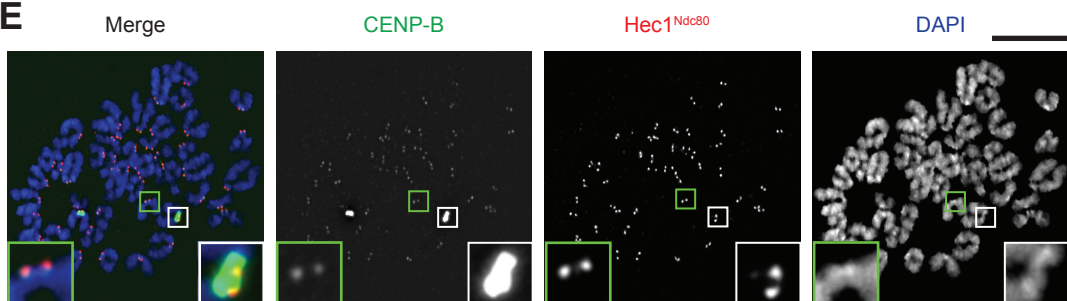
C



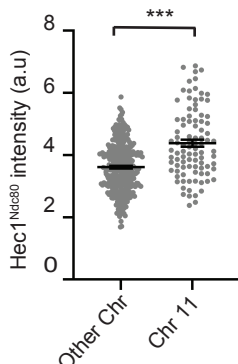
D



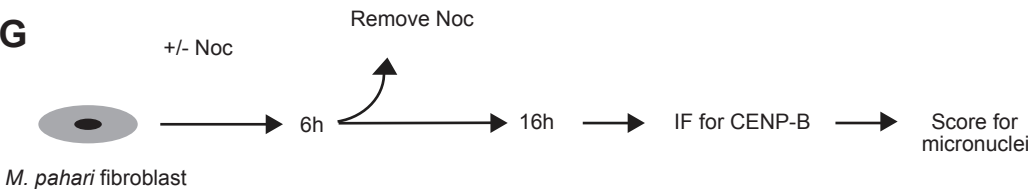
E



F



G



H

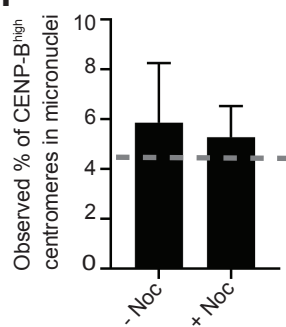
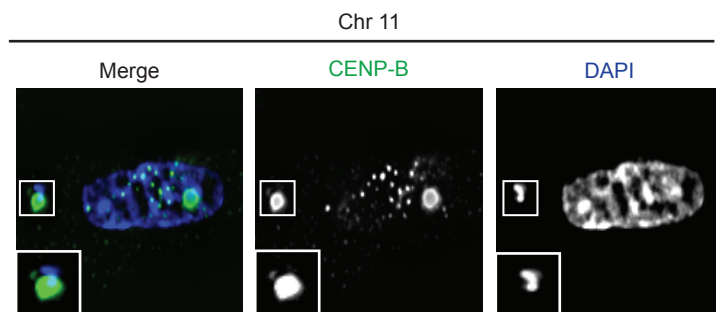
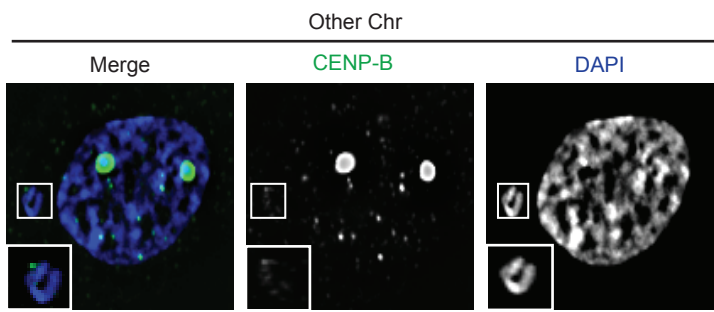
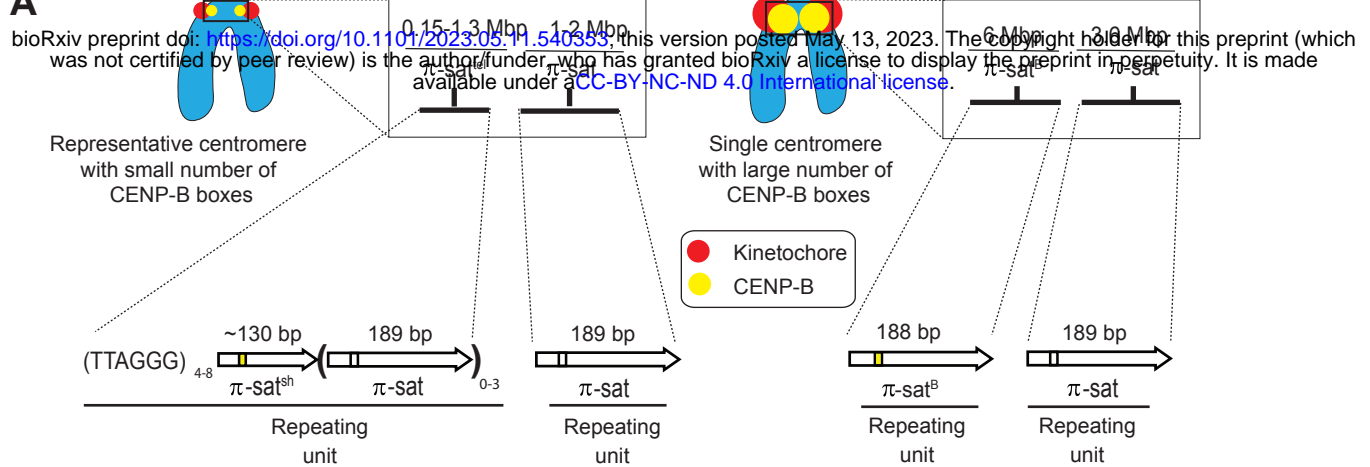


Figure 7

A



B

